



HAL
open science

Effective model for elastic waves propagating in a substrate supporting a dense array of plates/beams with flexural resonances

Jean-Jacques Marigo, Kim Pham, Agnès Maurel, Sebastien Guenneau

► To cite this version:

Jean-Jacques Marigo, Kim Pham, Agnès Maurel, Sebastien Guenneau. Effective model for elastic waves propagating in a substrate supporting a dense array of plates/beams with flexural resonances. *Journal of the Mechanics and Physics of Solids*, 2020, 143, pp.104029. 10.1016/j.jmps.2020.104029 . hal-02961904

HAL Id: hal-02961904

<https://ensta-paris.hal.science/hal-02961904>

Submitted on 15 Jul 2022

HAL is a multi-disciplinary open access archive for the deposit and dissemination of scientific research documents, whether they are published or not. The documents may come from teaching and research institutions in France or abroad, or from public or private research centers.

L'archive ouverte pluridisciplinaire **HAL**, est destinée au dépôt et à la diffusion de documents scientifiques de niveau recherche, publiés ou non, émanant des établissements d'enseignement et de recherche français ou étrangers, des laboratoires publics ou privés.



Distributed under a Creative Commons Attribution - NonCommercial 4.0 International License

Effective model for elastic waves propagating in a substrate supporting a dense array of plates/beams with flexural resonances

Jean-Jacques Marigo

*Laboratoire de Mécanique des solides, Ecole Polytechnique,
Route de Saclay, 91120 Palaiseau, France*

Kim Pham

*IMSIA, CNRS, EDF, CEA, ENSTA Paris, Institut Polytechnique de Paris,
828 Bd des Maréchaux, 91732 Palaiseau, France*

Agnès Maurel

*Institut Langevin, ESPCI Paris, Université PSL, CNRS,
1 rue Jussieu, Paris 75005, France*

Sébastien Guenneau

Aix Marseille Univ, CNRS, Centrale Marseille, Institut Fresnel, Marseille, France

Abstract

We consider the effect of an array of plates or beams over a semi-infinite elastic ground on the propagation of elastic waves hitting the interface. The plates/beams are slender bodies with flexural resonances at low frequencies able to perturb significantly the propagation of waves in the ground. An effective model is obtained using asymptotic analysis and homogenization techniques, which can be expressed in terms of the ground alone with effective dynamic (frequency-dependent) boundary conditions of the Robin's type. For an incident plane wave at oblique incidence, the displacement fields and the reflection coefficients are obtained in closed forms and their validity is inspected by comparison with direct numerics in a two-dimensional setting.

Keywords: asymptotic analysis; elastic waves; metamaterials; metasurfaces; multimodal method

2010 MSC: 00-01, 99-00

1. Introduction

2 We are interested in wave propagation in a semi-infinite elastic substrate supporting a peri-
3 dic and dense array of thin or slender bodies. This is the canonic idealized configuration used
4 to illustrate the problem of "site-city interaction". Such a problem, recent on the seismology
5 history scale, aims to account for the urban environment as a factor modifying the seismic ground
6 motion. Starting in the 19th century, the interest was primarily focused on the motion of the soil
7 elicited by static or dynamic sources being concentrated or distributed on the free surface in the
8 absence of buildings. These studies have led to important results as the Lamb's problem [1, 2].

Preprint submitted to Journal of the Mechanics and Physics of Solids

April 1, 2020

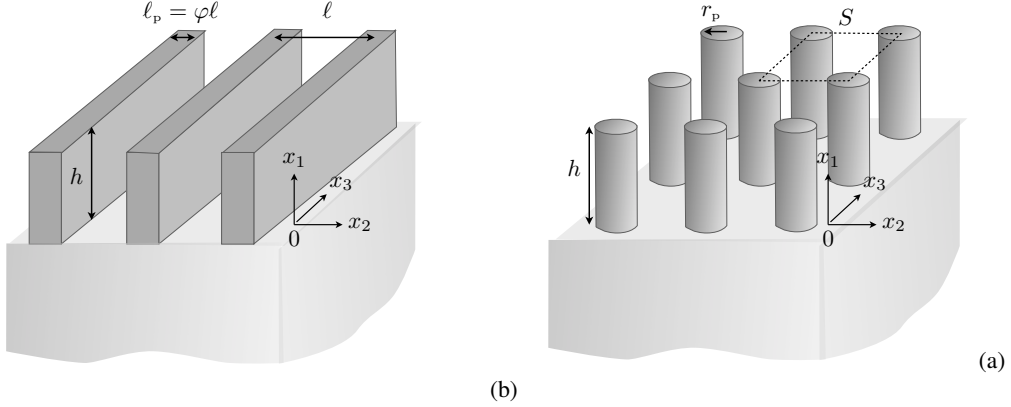


Figure 1: Geometry of the actual problems: (a) Array of parallel plates infinite along x_3 atop an isotropic substrate; (b) Doubly periodic array of cylindrical beams atop an isotropic substrate. The scalings are chosen to capture the bending resonances only; with k_T the wavenumber in the substrate, $k_T h = \eta$ and $k_T \ell = O(\eta^2)$.

9 Then, more realistic configurations have been considered using approximate models to predict
10 the effect of complex soils, including the presence of buried foundations, on the displacements
11 in structures on the ground, see *e.g.* [3, 4, 5] and [6] for a review. In the classical two-step
12 model, the displacements in the soil without structures above, so-called free fields, were firstly
13 calculated and they were subsequently used as input data to determine the motion within the
14 structure [4, 6]. This means that the interaction, referred to as the soil-structure interaction, was
15 restricted to the effect of the soil on the structure. In the mid-1970s, Luco and Contesse [7] and
16 Wong and Trifunac [8] studied the interaction between nearby buildings and they evidenced the
17 resulting modification on the ground motion. They termed this mutual interaction the structure-
18 soil-structure interaction, which has been later renamed soil-structure-soil interaction. On the
19 basis of these pioneering works the idea took root that several structures may interact with each
20 other and modify the ground motion, supplied by numerical simulations and direct observations
21 during earthquakes [9, 10, 11, 12, 13, 14, 15, 16]. At the scale of a city with the specificity of
22 the presence of a sedimentary basin, the soil-structure-soil interaction has been called site-city
23 interaction, a term first coined by Guéguen [10]. From a theoretical point of view, most of the
24 models encapsulate the response of a building with a single or multi-degree of freedom system
25 [17, 10, 18, 19, 20, 16]. On the basis of this model, Boutin, Roussillon and co-workers have
26 developed homogenized models where the multiple interactions between periodically located
27 oscillators are accounted for from a macroscopic city-scale point of view [19, 21, 22, 23, 24]. In
28 the low frequency limit, that is when the incident wavelength is large compared to the resonator
29 spacing, the effect of the resonators can be encapsulated in effective boundary conditions of
30 the Robin type for the soil, a result that we shall recover in the present study. Such a mass-
31 spring model has been used in physics for randomly distributed oscillators [25] and periodically
32 distributed oscillators [26, 27, 28] for their influence on surface Love and Rayleigh waves. The
33 ability of arrays of resonators to block Love and Rayleigh waves has been exploited to envision
34 new devices of seismic metasurfaces [29, 30, 31, 32, 33, 34, 35, 36, 37, 38, 39] in analogy with
35 metasurfaces in acoustics [40, 41] and in electromagnetism [42, 43].

In this study, we use asymptotic analysis and homogenization techniques to revisit the problem of the interaction of a periodic array of plates or beams on the propagation of seismic

waves in three dimensions. We consider slender bodies in the low frequency limit which means two things. Firstly, the typical wavelength $1/k$ is much larger than the array spacing ℓ , which is a classical hypothesis. Second, we focus on the lowest resonances of the bodies being flexural resonances. The first flexural resonances correspond to $kh \sim \ell_p/h$, with ℓ_p the body thickness, h the body height and h/ℓ_p the slenderness (in comparison the first longitudinal resonance appears at $kh \sim 1$). Now, we consider dense arrays, which means that $\ell_p \sim \ell$, and $\varphi = \ell_p/\ell \in (0, 1)$ (Figure 1). Hence the asymptotic analysis is conducted considering that

the wavelength $1/k$ is large compared to h which is itself large compared to $\ell_p \sim \ell$.

It is worth noting that assuming $\varphi = O(\eta^n)$ with $n \geq 1$ would allow a reduction of the model in a first step, resulting in concentrated force problems, as implicitly considered in [19, 21, 36]. Here on the contrary, the implementation of the asymptotic method will require that we reconstruct the asymptotic theory of plates and beams in a low frequency regime, as previously done for a single body in solid mechanics, see *e.g.* [44, 45] for plates and [46, 47, 48, 49] for beams. However, this classical theory has to be complemented with matched asymptotic expansions to link the behavior in the periodic set of bodies with that in the substrate. This “soil-structure” coupling requires a specific treatment as used in interface homogenization [50, 51, 52, 53], see also [54] for a resonant case. In the present case, we shall derive effective boundary and transmission conditions in a homogenized region which replaces the actual array; and in this effective region the wave equation for flexural waves applies. This problem can be further simplified in effective boundary conditions of the Robin type on the surface of the soil, namely

$$\boldsymbol{\sigma} \cdot \mathbf{n} = \mathbf{K}(\omega)\mathbf{u}, \quad (1)$$

36 where the frequency-dependent rigidity matrix \mathbf{K} depends explicitly on the flexural frequencies of
 37 the plates/beams. The rigidity matrix is diagonal as soon as the bodies have sufficient symmetry,
 38 resulting in effective impedance conditions which resemble those obtained in [22] in the same
 39 settings.

40 The paper is organized as follows. In §2, we summarize the result of the asymptotic ana-
 41 lysis in the case of an array of plates, whose detailed derivation is given in §3. The resulting
 42 “complete” formulation (3)-(5) is equivalent to that in (6)-(7) thanks to a partial resolution of
 43 the problem. In §4, the accuracy of the effective model is inspected by comparison with direct
 44 numerics based on multimodal method [55] for an in-plane incident wave. The strong coupling
 45 of the array with the ground at the flexural resonances is exemplified and the agreement between
 46 the actual and effective problems is discussed. We finish the study in §5 with concluding remarks
 47 and perspectives. A short comment on the solution in the region of the plates is given in Appendix
 48 A. We provide in Appendix B the effective problem for the an array of beams which is merely
 49 identical to the case of the plates with some specificities which are addressed.

50 2. The actual problem and the effective problem

51 We consider in this section the asymptotic analysis of an array of parallel plates atop an
 52 isotropic elastic substrate. We note that the problem splits in the in-plane and out-of-plane po-
 53 larizations. The latter case has been already addressed in [37]. We focus in this section on the
 54 former, in-plane, vector elastic case. We further note that the asymptotic analysis of a doubly
 55 periodic array of cylinders atop an isotropic substrate is a fully coupled elastodynamic wave
 56 problem, which is thus slightly more involved and addressed in Appendix B.

57 *2.1. The physical problem*

We consider the equation of elastodynamics for the displacement vector \mathbf{u} , the stress tensor $\boldsymbol{\sigma}$ and the strain tensor $\boldsymbol{\varepsilon}$

$$\left\{ \begin{array}{l} \text{in the substrate, } x_1 \in (-\infty, 0) : \quad \operatorname{div} \boldsymbol{\sigma} + \rho_s \omega^2 \mathbf{u} = \mathbf{0}, \quad \boldsymbol{\sigma} = 2\mu_s \boldsymbol{\varepsilon} + \lambda_s \operatorname{tr}(\boldsymbol{\varepsilon}) I, \quad \boldsymbol{\varepsilon} = \frac{1}{2}(\nabla \mathbf{u} + {}^t \nabla \mathbf{u}), \\ \text{in the plates, } x_1 \in (0, h) : \quad \operatorname{div} \boldsymbol{\sigma} + \rho_p \omega^2 \mathbf{u} = \mathbf{0}, \quad \boldsymbol{\sigma} = 2\mu_p \boldsymbol{\varepsilon} + \lambda_p \operatorname{tr}(\boldsymbol{\varepsilon}) I, \end{array} \right. \quad (2)$$

58 with the Lamé coefficients (λ_p, μ_p) of the plates and (λ_s, μ_s) of the substrate, ω the angular fre-
 59 quency and I stands for the identity matrix. In three dimensions with $\mathbf{x} = (x_1, x_2, x_3)$, stress free
 60 conditions $\boldsymbol{\sigma} \cdot \mathbf{n} = \mathbf{0}$ apply at each boundary between an elastic medium (the plates or the sub-
 61 strate) and air, with \mathbf{n} the normal to the interface. Eventually, the continuity of the displacement
 62 and of the normal stress apply at each boundary between the parallel plates and the substrate.
 63 This problem can be solved once the source \mathbf{u}^{inc} has been defined and accounting for the radia-
 64 tion condition when $x_1 \rightarrow -\infty$ which applies to the scattered field $(\mathbf{u} - \mathbf{u}^{\text{inc}})$.

65 *2.2. The effective problem*

66 Below we summarize the main results of the analysis developed in the §3, which provides the
 67 so-called “complete formulation” where the array of parallel plates is replaced by an equivalent
 68 layer associated with effective boundary and transmission conditions (Figure 2(a)). Owing to a
 69 partial resolution, this formulation can be simplified to an equivalent ”impedance formulation”
 70 set on the substrate on its own (Figure 2(b)).

71 *2.2.1. Complete formulation*

The effective problem reads as follow

$$\left\{ \begin{array}{l} \text{In the substrate, } x_1 \in (-\infty, 0) : \quad \operatorname{div} \boldsymbol{\sigma} + \rho_s \omega^2 \mathbf{u} = \mathbf{0}, \quad \boldsymbol{\sigma} = 2\mu_s \boldsymbol{\varepsilon} + \lambda_s \operatorname{tr}(\boldsymbol{\varepsilon}) I, \\ \text{In the region of the plates, } x_1 \in (0, h) : \quad \frac{\partial^4 u_2}{\partial x_1^4} - \kappa^4 u_2 = 0, \quad \kappa = \left(\frac{\rho_p \omega^2 \ell_p}{D_p} \right)^{1/4}, \\ \quad \quad \quad u_1(x_1, \mathbf{x}') = u_1(0, \mathbf{x}'), \quad u_3(x_1, \mathbf{x}') = u_3(0, \mathbf{x}'), \end{array} \right. \quad (3)$$

with $\mathbf{x}' = (x_2, x_3)$,

$$D_p = \frac{E_p}{(1 - \nu_p^2)} \frac{\ell_p^3}{12}, \quad (4)$$

the flexural rigidity of the plates (ρ_p the mass density, E_p the Young’s modulus and ν_p the Pois-
 son’s ratio). It is complemented with boundary conditions at $x_1 = 0$ and $x_1 = h$ of the form

$$\left\{ \begin{array}{l} \sigma_{11}(0^-, \mathbf{x}') = \rho_p \omega^2 \varphi h u_1(0, \mathbf{x}'), \quad \sigma_{12}(0^-, \mathbf{x}') = -\frac{D_p}{\ell} \frac{\partial^3 u_2}{\partial x_1^3}(0^+, \mathbf{x}'), \\ \sigma_{13}(0^-, \mathbf{x}') = \varphi h \left(E_p \frac{\partial^2 u_3}{\partial x_3^2}(0^-, \mathbf{x}') + \rho_p \omega^2 u_3(0^-, \mathbf{x}') \right), \\ u_2(0^+, \mathbf{x}') = u_2(0^-, \mathbf{x}'), \quad \frac{\partial u_2}{\partial x_1}(0^+, \mathbf{x}') = 0, \\ \frac{\partial^2 u_2}{\partial x_1^2}(h, \mathbf{x}') = \frac{\partial^3 u_2}{\partial x_1^3}(h, \mathbf{x}') = 0. \end{array} \right. \quad (5)$$

72 These effective conditions express (i) at $x_1 = 0$ a balance of the stress, prescribed displacements
 73 and vanishing rotation and (ii) at $x_1 = h$, free end conditions with vanishing bending moment
 74 and shearing force.

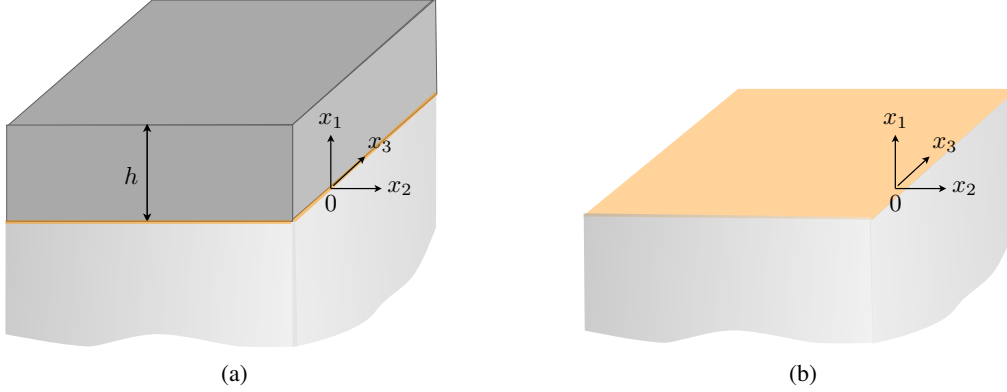


Figure 2: Geometry in the effective problems for an array of plates. (a) In the complete formulation, the region of the array is replaced by an equivalent layer where (3) applies, complemented by the transmission conditions in (5). (b) In the impedance formulation, the problem is reduced to effective boundary conditions (6) which hold at $x_1 = 0$. The same holds for the array of beams, with (a) (B.1)-(B.3) and (b) (B.5).

75 2.2.2. Impedance formulation

From (3), the problem in $x_1 \in (0, h)$ can be solved owing to the linearity of the problem with respect to $u_2(0^-, x_2)$, see Appendix A. Doing so, the problem can be thought in the substrate on its own along with the boundary conditions of the Robin's type, namely

$$\begin{cases} \operatorname{div} \boldsymbol{\sigma} + \rho_p \omega^2 \mathbf{u} = \mathbf{0}, & \boldsymbol{\sigma} = 2\mu_p \boldsymbol{\varepsilon} + \lambda_p \operatorname{tr}(\boldsymbol{\varepsilon}) \mathbf{I}, & x_1 \in (-\infty, 0), \\ \sigma_{11}(0, \mathbf{x}') = Z u_1(0, \mathbf{x}'), & \sigma_{12}(0, \mathbf{x}') = Z f(\kappa h) u_2(0, \mathbf{x}'), \\ \sigma_{13}(0, \mathbf{x}') = Z \left(\frac{E_p}{\rho_p \omega^2} \frac{\partial^2 u_3}{\partial x_3^2}(0, \mathbf{x}') + u_3(0, \mathbf{x}') \right), \end{cases} \quad (6)$$

with the following impedance parameters

$$Z = \rho_p \omega^2 \varphi h, \quad f(\kappa h) = \frac{\operatorname{sh} \kappa h \cos \kappa h + \operatorname{ch} \kappa h \sin \kappa h}{\kappa h (1 + \operatorname{ch} \kappa h \cos \kappa h)}, \quad (7)$$

76 (we have used that $D_p \kappa^4 = \rho_p \omega^2 \ell_p$). The conditions on $(\sigma_{11}, \sigma_{12})$ encapsulate the effects of the
 77 in-plane bending of the plates while the condition on σ_{13} can be viewed as the linear momentum
 78 of an axially loaded bar (in the absence of substrate, we recover the wave equation for quasi-
 79 longitudinal waves). It is worth noting that for out-of-plane displacements, $u_3(x_1, x_2)$ and $u_1 =$
 80 $u_2 = 0$, the boundary conditions simplify to $\sigma_{13}(0, x_2) = \rho_p \omega^2 \varphi h u_3(0, x_2)$. This corresponds
 81 to the impedance condition $\sigma_{13}(0, x_2) = \mu_p \varphi \omega \sqrt{\rho_p / \mu_p} \tan(\omega h \sqrt{\rho_p / \mu_p}) u_3(0, x_2)$ used in [37] and
 82 obtained here in the low-frequency limit $\omega h \sqrt{\rho_p / \mu_p} \ll 1$.

83 3. Derivation of the effective problem

As previously said, the asymptotic analysis is conducted considering that the typical wavelength $1/k$ is large compared to the plate height h which is itself large compared to the array spacing $\ell \sim \ell_p$. Hence, with $k_T = \omega \sqrt{\rho_s/\mu_s}$ and $k_L = \omega \sqrt{\rho_s/(\lambda_s + 2\mu_s)}$ of the same order of magnitude, we define the small non-dimensional parameter η as

$$\eta = \sqrt{k_T \ell}, \quad \text{and} \quad k_T h = O(\eta),$$

(note that to excite both the bending and the longitudinal modes another scaling is required with $kh = O(1)$, and this is a higher frequency regime studied in [36]). Accordingly, the asymptotic analysis is conducted using the rescaled height \hat{h} of the plates and array's spacing $\hat{\ell}$ defined by

$$(\hat{h}, \hat{\ell}) = \left(\frac{h}{\eta}, \frac{\ell}{\eta^2} \right),$$

which models an array of densely packed thin plates. We also define the associated rescaled spatial coordinates

$$y_1 = \frac{x_1}{\eta}, \quad \mathbf{z} = \frac{(x_1, x_2)}{\eta^2}. \quad (8)$$

84 3.1. Effective wave equation in the region of the plates

85 3.1.1. Notations

In the region of the array of plates, the displacements and the stresses vary in the horizontal direction over small distances dictated by ℓ , and over large distances dictated by the incoming waves; these two scales are accounted for by the two-scale coordinates (\mathbf{x}', z_2) , with $\mathbf{x}' = (x_2, x_3)$. In the vertical direction, the variations are dictated by h only and this is accounted for by the rescaled coordinate y_1 . It follows that the fields $(\mathbf{u}, \boldsymbol{\sigma})$ are written in the form

$$\mathbf{u} = \sum_{n \geq 0} \eta^n \mathbf{w}^n(y_1, z_2, \mathbf{x}'), \quad \boldsymbol{\sigma} = \sum_{n \geq 0} \eta^n \boldsymbol{\pi}^n(y_1, z_2, \mathbf{x}'), \quad (9)$$

with the three-scale differential operator reading

$$\nabla \rightarrow \frac{\mathbf{e}_1}{\eta} \frac{\partial}{\partial y_1} + \frac{\mathbf{e}_2}{\eta^2} \frac{\partial}{\partial z_2} + \nabla_{\mathbf{x}'}, \quad (10)$$

where $\mathbf{e}_1 = (1, 0, 0)$ and $\mathbf{e}_2 = (0, 1, 0)$. Now, we introduce the strain tensor with respect to \mathbf{x}'

$$\boldsymbol{\varepsilon}^{\mathbf{x}'}(\mathbf{u}) = \frac{1}{2} \begin{pmatrix} 0 & \partial_{x_2} u_1 & \partial_{x_3} u_1 \\ \partial_{x_2} u_1 & 2\partial_{x_2} u_2 & (\partial_{x_3} u_2 + \partial_{x_2} u_3) \\ \partial_{x_3} u_1 & (\partial_{x_3} u_2 + \partial_{x_2} u_3) & 2\partial_{x_3} u_3 \end{pmatrix}, \quad (11)$$

and the strain tensors with respect to the rescaled coordinates y_1 and z_2 ,

$$\boldsymbol{\varepsilon}^{y_1}(\mathbf{u}) = \frac{1}{2} \begin{pmatrix} 2\partial_{y_1} w_1 & \partial_{y_1} u_2 & \partial_{y_1} u_3 \\ \partial_{y_1} u_2 & 0 & 0 \\ \partial_{y_1} u_3 & 0 & 0 \end{pmatrix}, \quad \boldsymbol{\varepsilon}^{z_2}(\mathbf{u}) = \frac{1}{2} \begin{pmatrix} 0 & \partial_{z_2} u_1 & 0 \\ \partial_{z_2} u_1 & 2\partial_{z_2} u_2 & \partial_{z_2} u_3 \\ 0 & \partial_{z_2} u_3 & 0 \end{pmatrix}. \quad (12)$$

The system in the region of the plates reads, from (2),

$$\left\{ \begin{array}{l} \text{(E}_1\text{)} \quad \frac{1}{\eta^2} \partial_{z_2} \sigma_{12} + \frac{1}{\eta} \partial_{y_1} \sigma_{11} + \partial_{x_\alpha} \sigma_{1\alpha} + \rho_p \omega^2 u_1 = 0, \\ \text{(E}_\alpha\text{)} \quad \frac{1}{\eta^2} \partial_{z_2} \sigma_{\alpha 2} + \frac{1}{\eta} \partial_{y_1} \sigma_{\alpha 1} + \partial_{x_\beta} \sigma_{\alpha\beta} + \rho_p \omega^2 u_\alpha = 0, \\ \text{(C)} \quad \sigma = \frac{1}{\eta^2} (2\mu_p \boldsymbol{\varepsilon}^{z_2} + \lambda_p \text{tr}(\boldsymbol{\varepsilon}^{z_2})) + \frac{1}{\eta} (2\mu_p \boldsymbol{\varepsilon}^{y_1} + \lambda_p \text{tr}(\boldsymbol{\varepsilon}^{y_1})) + (2\mu_p \boldsymbol{\varepsilon}^{\mathbf{x}'} + \lambda_p \text{tr}(\boldsymbol{\varepsilon}^{\mathbf{x}'})), \end{array} \right. \quad (13)$$

where repeated indices means summation, and with the convention on the Greek letters $\alpha, \beta = 2, 3$. In the above relation, $\boldsymbol{\varepsilon}$ stands for $\boldsymbol{\varepsilon}(\mathbf{u})$. We shall use the stress-strain relation written in the inverse form

$$\text{(C')} \quad \frac{1}{\eta^2} \boldsymbol{\varepsilon}^{z_2} + \frac{1}{\eta} \boldsymbol{\varepsilon}^{y_1} + \boldsymbol{\varepsilon}^{\mathbf{x}'} = \frac{(1 + \nu_p)}{E_p} \boldsymbol{\sigma} - \frac{\nu_p}{E_p} \text{tr}(\boldsymbol{\sigma}) I. \quad (14)$$

Eventually, the boundary conditions read

$$\sigma_{2i} = 0, \quad i = 1, 2, 3, \quad \text{at } z_2 = \pm \varphi \hat{\ell} / 2, \quad (15)$$

and are complemented by boundary conditions at $y_1 = 0, \hat{h}$ assumed to be known (they will be justified later). We seek to establish the effective behaviour in the region of the array in terms of macroscopic averaged fields which do not depend anymore on the rapid coordinate z_2 associated with the small scale $\hat{\ell}$ as the following averages taken along rescaled variable z_2 . These averaged fields are defined at any order n as

$$\overline{\mathbf{w}^n}(y_1, \mathbf{x}') = \frac{1}{\varphi \hat{\ell}} \int_Y \mathbf{w}^n(y_1, z_2, \mathbf{x}') dz_2, \quad \overline{\boldsymbol{\pi}^n}(y_1, \mathbf{x}') = \frac{1}{\hat{\ell}} \int_Y \boldsymbol{\pi}^n(y_1, z_2, \mathbf{x}') dz_2,$$

⁸⁶ with $Y = \{z_2 \in (-\varphi \hat{\ell} / 2, \varphi \hat{\ell} / 2)\}$ the segment shown in figure 3.

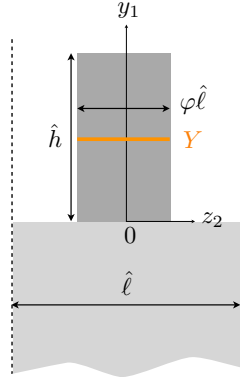


Figure 3: Analysis of a single plate in rescaled coordinates, (9) with $Y = \{z_2 \in (-\varphi \hat{\ell} / 2, \varphi \hat{\ell} / 2)\}$; the analysis holds within the plate far from its boundaries at $y_1 = 0, \hat{h}$.

87 *3.1.2. Sequence of resolution and main results of the analysis*

88 We shall derive the equation satisfied in the region of the array, and additional results on the
 89 stresses $(\overline{\pi_{1i}^0}, \overline{\pi_{1i}^1})$, $i = 1, 2, 3$, required to establish the effective boundary conditions at $y_1 = 0, \hat{h}$.
 90 The main results will be obtained following the procedure :

1. We establish the following properties on π^0

$$\overline{\pi_{11}^0} = 0, \quad \pi_{2i}^0 = 0, \quad i = 1, 2, 3, \quad \overline{\pi_{13}^0} = 0. \quad (16)$$

2. Then we derive the dependence of $(\mathbf{w}^0, \mathbf{w}^1)$ on z_2 which have the form

$$\begin{cases} w_1^0 = W_1^0(\mathbf{x}'), & w_2^0 = W_2^0(y_1, \mathbf{x}'), & w_3^0 = W_3^0(\mathbf{x}'), \\ w_1^1 = W_1^1(\mathbf{x}') - \frac{\lambda_p}{2(\lambda_p + \mu_p)} \frac{\partial W_3^0}{\partial x_3}(\mathbf{x}') y_1 - \frac{\partial W_2^0}{\partial y_1}(y_1, \mathbf{x}') z_2, & w_\alpha^1 = W_\alpha^1(y_1, \mathbf{x}'), \end{cases} \quad (17)$$

and

$$\pi_{11}^0 = -\frac{E_p}{1 - \nu_p^2} \frac{\partial^2 W_2^0}{\partial y_1^2}(y_1, \mathbf{x}') z_2, \quad \overline{\pi_{33}^0} = \varphi E_p \frac{\partial W_3^0}{\partial x_3}(\mathbf{x}'). \quad (18)$$

3. Eventually, we identify the form of $\overline{\pi_{1i}^1}$, $i = 1, 2, 3$, and the Euler -Bernoulli equation governing the bending W_2^0 . Specifically

$$\begin{cases} \overline{\pi_{11}^1}(y_1, \mathbf{x}') = \rho_p \omega^2 \varphi W_1^0(\mathbf{x}') (\hat{h} - y_1), \\ \overline{\pi_{12}^1}(y_1, \mathbf{x}') = -\frac{E_p}{(1 - \nu_p^2)} \frac{\varphi^3 \hat{\ell}^2}{12} \frac{\partial^3 W_2^0}{\partial y_1^3}(y_1, \mathbf{x}'), \\ \overline{\pi_{13}^1}(y_1, \mathbf{x}') = \varphi \left(E_p \frac{\partial^2 W_3^0}{\partial x_3^2}(\mathbf{x}') + \rho_p \omega^2 W_3^0(\mathbf{x}') \right) (\hat{h} - y_1), \end{cases} \quad (19)$$

and

$$\frac{E_p}{(1 - \nu_p^2)} \frac{\varphi^2 \hat{\ell}^2}{12} \frac{\partial^4 W_2^0}{\partial y_1^4} - \rho_p \omega^2 W_2^0 = 0. \quad (20)$$

91

92 In the remainder of this section, we shall establish the above results. We shall denote $(E_1)^n$, $(E_\alpha)^n$
 93 and $(C)^n$ the equations which correspond to terms in (13) factor of η^n .

94 *3.1.3. First step: properties of π^0 in (16)*

95 From $(E_1)^{-2}$ and $(E_\alpha)^{-2}$ in (13), we have that $\partial_{z_2} \pi_{12}^0 = 0$, $i = 1, 2, 3$, which along with the
 96 boundary conditions at $z_2 = \pm \varphi \hat{h}/2$ leave us with $\pi_{2i}^0 = 0$. Next from $(E_1)^{-1}$ and $(E_3)^{-1}$, we
 97 also have that $\partial_{y_1} \pi_{11}^0 + \partial_{z_2} \pi_{12}^0 = 0$ and $\partial_{y_1} \pi_{13}^0 + \partial_{z_2} \pi_{23}^0 = 0$; by averaging these relations over Y
 98 and accounting for $\pi_{2i}^1|_{\partial Y} = 0$, we get that $\overline{\pi_{11}^0}$ and $\overline{\pi_{13}^0}$ do not depend on y_1 . We now anticipate
 99 the boundary condition $\overline{\pi_{11}^0}(\hat{h}, \mathbf{x}') = \overline{\pi_{13}^0}(\hat{h}, \mathbf{x}') = 0$ that we shall prove later on (see forthcoming
 100 (54)), we get $\overline{\pi_{11}^0} = \overline{\pi_{13}^0} = 0$ in Y . We have the properties announced in (16).

101 3.1.4. *Second step: $(\mathbf{w}^0, \mathbf{w}^1)$ in (17) and $(\pi_{11}^0, \overline{\pi_{33}^0})$ in (18)*

Some of the announced results are trivially obtained. From $(C')^{-2}$ in (14) along with $\boldsymbol{\varepsilon}^{z_2}$ in (12), we get that $\partial_{z_2} w_i^0 = 0$, $i = 1, 2, 3$. From $(C'_{11})^{-1}$ and $(C'_{13})^{-1}$ along with $\boldsymbol{\varepsilon}^{z_2}$ and $\boldsymbol{\varepsilon}^{y_1}$ in (12), we also get that $\partial_{y_1} w_1^0 = \partial_{y_1} w_3^0 = 0$. This leaves us with the form of \mathbf{w}^0 in (17). Next $(C'_{\alpha\alpha})^{-1}$ tells us that $\partial_{z_2} w_\alpha^1 = 0$, in agreement with the form of w_α^1 in (17). We have yet to derive the form of w_1^1 , which is more demanding. From $(C'_{12})^{-1}$, $\partial_{z_2} w_1^1 = -\partial_{y_1} w_2^0$ and thus

$$w_1^1 = W_1(y_1, \mathbf{x}') - \frac{\partial W_2^0}{\partial y_1}(y_1, \mathbf{x}') z_2, \quad (21)$$

but we can say more on W_1 . Let us consider the system provided by $(C_{11})^0$ and $(C_{22})^0$, specifically

$$\begin{cases} \pi_{11}^0 = (\lambda_p + 2\mu_p)\partial_{y_1} w_1^1 + \lambda_p (\partial_{x_\alpha} w_\alpha^0 + \partial_{z_2} w_2^0), \\ 0 = (\lambda_p + 2\mu_p)(\partial_{x_2} w_2^0 + \partial_{z_2} w_2^0) + \lambda_p (\partial_{x_3} w_3^0 + \partial_{y_1} w_1^1), \end{cases} \quad (22)$$

where we have used that $\pi_{22}^0 = 0$. After elimination of $\partial_{z_2} w_2^0$ and owing to the form of w_α^0 in (16) and that of w_1^1 in (21) (at this stage), we get $\pi_{11}^0 = a(y_1, \mathbf{x}') z_2 + b(y_1, \mathbf{x}')$ with

$$a = -\frac{E_p}{1 - \nu_p^2} \frac{\partial^2 W_2^0}{\partial y_1^2}(y_1, \mathbf{x}'), \quad b = \frac{2\mu_p}{(\lambda_p + 2\mu_p)} \left(2(\lambda_p + \mu_p) \frac{\partial W_1}{\partial y_1}(y_1, \mathbf{x}') + \lambda_p \frac{\partial W_3^0}{\partial x_3}(\mathbf{x}') \right), \quad (23)$$

(we have used that $E_p/(1 - \nu_p^2) = 4\mu_p(\mu_p + \lambda_p)/(\lambda_p + 2\mu_p)$). It is sufficient to remark that $\overline{\pi_{11}^0} = 0$ imposes $b = 0$ which provides $\pi_{11}^0 = a z_2$ as announced in (18). We also get

$$W_1(y_1, \mathbf{x}') = W_1^1(\mathbf{x}') - \frac{\lambda_p}{2(\lambda_p + \mu_p)} \frac{\partial W_3^0}{\partial x_3}(\mathbf{x}') y_1, \quad (24)$$

which along with (21) leaves us with the form of w_1^1 in (17). The same procedure is used to get π_{33}^0 which, from $(C_{33})^0$, reads

$$\pi_{33}^0 = (\lambda_p + 2\mu_p)\partial_{x_3} w_3^0 + \lambda_p (\partial_{y_1} w_1^1 + \partial_{x_2} w_2^0 + \partial_{z_2} w_2^0). \quad (25)$$

Using that $\pi_{22}^0 = 0$ to eliminate $\partial_{z_2} w_2^0$, we get

$$\pi_{33}^0 = E_p \frac{\partial W_3^0}{\partial x_3}(\mathbf{x}') - \frac{2\mu_p \lambda_p}{\lambda_p + 2\mu_p} \frac{\partial^2 W_2^0}{\partial y_1^2}(y_1, \mathbf{x}') z_2, \quad (26)$$

which after integration over Y leaves us with $\overline{\pi_{33}^0} = \varphi E_p \frac{\partial W_3^0}{\partial x_3}(\mathbf{x}')$ as announced in (18). Incidentally, w_2^0 can be determined from (22) and we find

$$w_2^0 = -\left(\frac{\partial W_2^0}{\partial x_2}(y_1, \mathbf{x}') + \frac{\lambda_p}{2(\lambda_p + \mu_p)} \frac{\partial W_3^0}{\partial x_3}(\mathbf{x}') \right) z_2 + \frac{\lambda_p}{\lambda_p + 2\mu_p} \frac{\partial^2 W_2^0}{\partial y_1^2} \frac{z_2^2}{2} + W_2^2(y_1, \mathbf{x}'). \quad (27)$$

102 3.1.5. *Third step: the $\overline{\pi_{1i}^1}$ in (19) and the Euler-Bernoulli equation in (20).*

We start with $(E_1)^0$ and $(E_\alpha)^0$ in (13) integrated over Y , specifically,

$$\frac{\partial \overline{\pi_{11}^1}}{\partial y_1} + \rho_p \omega^2 \varphi W_1^0 = 0, \quad \frac{\partial \overline{\pi_{12}^1}}{\partial y_1} + \rho_p \omega^2 \varphi W_2^0 = 0, \quad \frac{\partial \overline{\pi_{13}^1}}{\partial y_1} + \frac{\partial \overline{\pi_{33}^0}}{\partial x_3} + \rho_p \omega^2 W_3^0 = 0, \quad (28)$$

103 where we have used $\overline{\pi_{1\alpha}^0} = 0$ from (16) and $\boldsymbol{\pi}^2 \cdot \mathbf{n}_{|\partial Y} = \mathbf{0}$. Since W_1^0 and W_3^0 depend on \mathbf{x}' only,
 104 and accounting for $\overline{\pi_{33}^0}(\mathbf{x}') = \varphi E_p \frac{\partial W_3^0}{\partial x_3}(\mathbf{x}')$ from (18), we get by integration the forms of $\overline{\pi_{11}^1}$ and
 105 $\overline{\pi_{13}^1}$ announced in (19). Note that we have anticipated the boundary conditions $\overline{\pi_{1i}^1} = 0$ at $y_1 = \hat{h}$,
 106 see forthcoming (54).

The equation on $\overline{\pi_{12}^1}$ in (28) will provide the Euler-Bernoulli equation once $\overline{\pi_{12}^1}$ has been determined (the integration is not possible since W_2^0 depends on y_1). To do so, we use, that $\partial_{y_1} \pi_{11}^0 + \partial_{z_2} \pi_{12}^1 = 0$, from $(E_1)^{-1}$ in (13), along with $\pi_{11}^0 = -\frac{E_p}{1-\nu_p^2} \frac{\partial^2 W_2^0}{\partial y_1^2}(y_1, \mathbf{x}') z_2$ from (18). After integration and using the boundary condition of vanishing π_{12}^1 at $z_2 = \pm \varphi \hat{\ell}/2$, we get that

$$\pi_{12}^1 = \frac{E_p}{2(1-\nu_p^2)} \frac{\partial^3 W_1^0}{\partial y_1^3}(y_1, \mathbf{x}') \left(z_2^2 - \frac{\varphi^2 \hat{\ell}^2}{4} \right), \quad (29)$$

107 hence the form of $\overline{\pi_{12}^1}$ in (19). It is now sufficient to use π_{12}^1 in (28) to get the Euler-Bernoulli
 108 announced in (20).

109 3.2. *Effective boundary conditions at the top of the array*

To derive the transmission conditions at the top of the array, we perform a zoom by substituting y_1 used in (9) by $z_1 = y_1/\eta$, see Figure 4a. Accordingly, the expansions of the fields are sought of the form

$$\mathbf{u} = \sum_{n \geq 0} \eta^n \mathbf{v}^n(\mathbf{z}, \mathbf{x}'), \quad \boldsymbol{\sigma} = \sum_{n \geq 0} \eta^n \boldsymbol{\tau}^n(\mathbf{z}, \mathbf{x}'), \quad (30)$$

where we denote $\mathbf{z} = (z_1, z_2)$. The coordinate $z_1 \in (-\infty, 0)$ accounts for small scale variations of the evanescent fields at the top of the plates. Next, the boundary conditions will be obtained by matching the solution in (30) for $z_1 \rightarrow -\infty$ with that in (9), valid far from the boundary, for $y_1 \rightarrow \hat{h}$. This means that we ask the two expansions to satisfy

$$\mathbf{v}^0(z_1, z_2, \mathbf{x}') + \eta \mathbf{v}^1(z_1, z_2, \mathbf{x}') + \dots \underset{z_1 \rightarrow -\infty}{\sim} \mathbf{w}^0(\hat{h} + \eta z_1, z_2, \mathbf{x}') + \eta \mathbf{w}^1(\hat{h} + \eta z_1, z_2, \mathbf{x}') + \dots,$$

(and the same for the stress tensors); note that we have used that $y_1 = \eta z_1$. It results that

$$\left\{ \begin{array}{l} \lim_{z_1 \rightarrow -\infty} \mathbf{v}^0(\mathbf{z}, \mathbf{x}') = \mathbf{w}^0(\hat{h}, z_2, \mathbf{x}'), \quad \lim_{z_1 \rightarrow -\infty} \left(\mathbf{v}^1(\mathbf{z}, \mathbf{x}') - z_1 \frac{\partial \mathbf{w}^0}{\partial y_1}(\hat{h}, z_2, \mathbf{x}') \right) = \mathbf{w}^1(\hat{h}, z_2, \mathbf{x}'), \\ \lim_{z_1 \rightarrow -\infty} \boldsymbol{\tau}^0(\mathbf{z}, \mathbf{x}') = \boldsymbol{\pi}^0(\hat{h}, z_2, \mathbf{x}'), \quad \lim_{z_1 \rightarrow -\infty} \left(\boldsymbol{\tau}^1(\mathbf{z}, \mathbf{x}') - z_1 \frac{\partial \boldsymbol{\pi}^0}{\partial y_1}(\hat{h}, z_2, \mathbf{x}') \right) = \boldsymbol{\pi}^1(\hat{h}, z_2, \mathbf{x}'). \end{array} \right. \quad (31)$$

110 According to the dependence of the fields in (30) on $(\mathbf{z}, \mathbf{x}')$, the differential operator reads as follows

$$\nabla \rightarrow \frac{1}{\eta^2} \nabla_{\mathbf{z}} + \nabla_{\mathbf{x}'}, \quad (32)$$

and we shall need only the first equation of (2), which reads

$$(e) \quad \frac{1}{\eta^2} \operatorname{div}_{\mathbf{z}} \boldsymbol{\sigma} + \operatorname{div}_{\mathbf{x}'} \boldsymbol{\sigma} + \rho_p \omega^2 \mathbf{u} = \mathbf{0}, \quad (33)$$

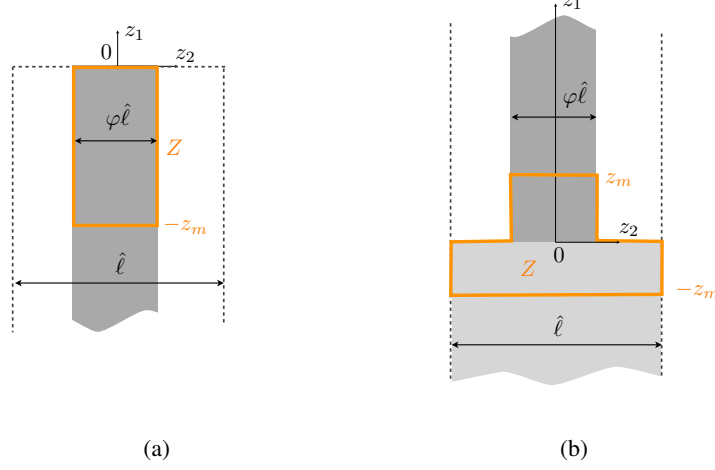


Figure 4: Analysis of the effective conditions at the top and at the bottom of the array. (a) Half strip at the top of the array in $\mathbf{z} = (z_1, z_2)$ coordinate with $z_1 \in (-\infty, 0)$, (b) Strip at the bottom of the array with $z_1 \in (-\infty, +\infty)$; for $z_1 \in (-\infty, 0)$, the terms in the expansions (30) are periodic with respect to $z_2 \in (-\hat{\ell}/2, \hat{\ell}/2)$.

where $\text{div}_{\mathbf{z}}$ and $\text{div}_{\mathbf{x}'}$ mean the divergence with respect to the coordinate \mathbf{z} and \mathbf{x}' respectively. In (33), $(e)^{-2}$ and $(e)^{-1}$ tell us that $\text{div}_{\mathbf{z}} \boldsymbol{\tau}^0 = \text{div}_{\mathbf{z}} \boldsymbol{\tau}^1 = \mathbf{0}$, that we integrate over $Z = \{z_1 \in (-z_m, 0), z_2 \in Y\}$ to get $\int_{\partial Z} \boldsymbol{\tau}^0 \cdot \mathbf{n} \, ds = \int_{\partial Z} \boldsymbol{\tau}^1 \cdot \mathbf{n} \, ds = \mathbf{0}$. On ∂Z (see figure 4(a)), $\boldsymbol{\tau}^0 \cdot \mathbf{n}$ and $\boldsymbol{\tau}^1 \cdot \mathbf{n}$ vanish except on the bottom edge Y of ∂Z at $z_1 = -z_m$ where $\mathbf{n} = -\mathbf{e}_1$. It follows, from (31) along with $\overline{\pi_{1i}^0} = 0$ in (16), that

$$\mathbf{0} = \lim_{z_m \rightarrow \infty} \int_{\partial Z} \boldsymbol{\tau}^0 \cdot \mathbf{n} \, ds = -\hat{\ell} \overline{\pi_{1i}^0}(\hat{h}, \mathbf{x}') \mathbf{e}_i, \quad \mathbf{0} = \lim_{z_m \rightarrow \infty} \int_{\partial Z} \boldsymbol{\tau}^1 \cdot \mathbf{n} \, ds = -\hat{\ell} \overline{\pi_{1i}^1}(\hat{h}, \mathbf{x}') \mathbf{e}_i, \quad (34)$$

which provides the boundary conditions

$$\overline{\pi_{1i}^0}(\hat{h}, \mathbf{x}') = \overline{\pi_{1i}^1}(\hat{h}, \mathbf{x}') = 0, \quad i = 1, 2, 3. \quad (35)$$

The conditions on $\overline{\pi_{1i}^0}$ are consistent with (16). The conditions on $\overline{\pi_{11}^1}$ and $\overline{\pi_{13}^1}$ are those anticipated in the previous section, see (19). Eventually, the condition $\overline{\pi_{12}^1}(\hat{h}, x_2) = 0$ along with the form of $\overline{\pi_{12}^1}$ in (19) leads to the condition of zero shear force

$$\frac{\partial^3 W_2^0}{\partial y_1^3}(\hat{h}, \mathbf{x}') = 0. \quad (36)$$

We have yet to derive the condition of zero bending moment. First, integrating $\text{div}_{\mathbf{z}} \boldsymbol{\tau}^0$ over Z , we get $0 = \int_{\partial Z} \tau_{ij}^0 n_j \, dz_2 = \int_Y \tau_{i1}^0|_{z_1=-z_m} \, dz_2$. Next, integrating over Z the scalar quantity $\mathbf{a} \cdot \text{div}_{\mathbf{z}} \boldsymbol{\tau}^0 = a_i \partial_{z_j} \tau_{ij}^0 = 0$ (since $\text{div}_{\mathbf{z}} \boldsymbol{\tau}^0 = \mathbf{0}$) with $\mathbf{a} = z_2 \mathbf{e}_1 - z_1 \mathbf{e}_2$ and further integrating by parts, we get that

$$0 = \int_{\partial Z} a_i \tau_{ij}^0 n_j \, ds = - \int_Y z_2 \tau_{11}^0|_{z_1=-z_m} \, dz_2 - z_m \int_Y \tau_{12}^0|_{z_1=-z_m} \, dz_2 = - \int_Y z_2 \tau_{11}^0|_{z_1=-z_m} \, dz_2, \quad (37)$$

(the integral on ∂Z reduces to that on Y at $z = -z_m$). From (31), when $z_m \rightarrow +\infty$, $\int_Y z_2 \tau_{11|z_1=-z_m}^0 \rightarrow \overline{z_2 \pi_{11}^0}(\hat{h}, \mathbf{x}')$ and, with $\pi_{11}^0 = -\frac{E_p}{1-\nu_p} \frac{\partial^2 W_2^0}{\partial y_1^2}(y_1, \mathbf{x}')$ from (18), we obtain the boundary condition

$$\frac{\partial^2 W_2^0}{\partial y_1^2}(\hat{h}, \mathbf{x}') = 0. \quad (38)$$

3.3. Effective transmission conditions between the substrate and the region of the array

To begin with, we shall need the solution valid in the substrate far from the interface at $y_1 = 0$; this solution is expanded as

$$\mathbf{u} = \sum_{n \geq 0} \eta^n \mathbf{u}^n(\mathbf{x}), \quad \boldsymbol{\sigma}(\mathbf{x}) = \sum_{n \geq 0} \eta^n \boldsymbol{\sigma}^n(\mathbf{x}), \quad (39)$$

with no dependence on the rapid coordinates, while in the array it is given by (9). As in the previous section, a zoom is performed in the vicinity of the interface between the substrate and the region of the array, owing to the substitution $y_1 \rightarrow z_1$. In the intermediate region, the fields are expanded as in (30) with the interface at $z_1 = 0$ and $z_1 \in (-\infty, +\infty)$, see Figure 4(b). It is worth noting that for $z_1 \in (-\infty, 0)$ the terms in the expansion (30) are assumed to be periodic with respect to $z_2 \in (-\hat{\ell}/2, \hat{\ell}/2)$ while for $z_1 \in (0, \infty)$ we have $z_2 \in (-\varphi\hat{\ell}/2, \varphi\hat{\ell}/2)$. Note that in principle we should use different notations for the expansions and for z_1 since their meaning is different; for simplicity, we keep the same notations. The transmission conditions will be obtained by matching the solution in (30) for $z_1 \rightarrow +\infty$ with that in (9) for $x_1 \rightarrow 0^+$, and for $z_1 \rightarrow -\infty$ with that in (39) for $x_1 \rightarrow 0^-$. Matching the solutions hence means (with $\mathbf{z} = (z_1, z_2)$ and $\mathbf{x}' = (x_2, x_3)$),

$$\begin{cases} \mathbf{v}^0(\mathbf{z}, \mathbf{x}') + \eta \mathbf{v}^1(\mathbf{z}, \mathbf{x}') + \cdots \underset{z_1 \rightarrow -\infty}{\sim} \mathbf{u}^0(\eta^2 z_1, \mathbf{x}') + \eta \mathbf{u}^1(\eta^2 z_1, \mathbf{x}') + \cdots, \\ \mathbf{v}^0(\mathbf{z}, \mathbf{x}') + \eta \mathbf{v}^1(\mathbf{z}, \mathbf{x}') + \cdots \underset{z_1 \rightarrow +\infty}{\sim} \mathbf{w}^0(\eta z_1, z_2, \mathbf{x}') + \eta \mathbf{w}^1(\eta z_1, z_2, \mathbf{x}') + \cdots, \end{cases}$$

where we have used that $x_1 = \eta^2 z_1$ and $y_1 = \eta z_1$. It results that

$$\begin{cases} \lim_{z_1 \rightarrow -\infty} \mathbf{v}^0(\mathbf{z}, \mathbf{x}') = \mathbf{u}^0(0^-, \mathbf{x}'), & \lim_{z_1 \rightarrow -\infty} \mathbf{v}^1(\mathbf{z}, \mathbf{x}') = \mathbf{u}^1(0^-, \mathbf{x}'), \\ \lim_{z_1 \rightarrow -\infty} \boldsymbol{\tau}^0(\mathbf{z}, \mathbf{x}') = \boldsymbol{\sigma}^0(0^-, \mathbf{x}'), & \lim_{z_1 \rightarrow -\infty} \boldsymbol{\tau}^1(\mathbf{z}, \mathbf{x}') = \boldsymbol{\sigma}^1(0^-, \mathbf{x}'), \end{cases} \quad (40)$$

and that

$$\begin{cases} \lim_{z_1 \rightarrow +\infty} \mathbf{v}^0(\mathbf{z}, \mathbf{x}') = \mathbf{w}^0(0^+, z_2, \mathbf{x}'), & \lim_{z_1 \rightarrow +\infty} \left(\mathbf{v}^1(\mathbf{z}, \mathbf{x}') - z_1 \frac{\partial \mathbf{w}^0}{\partial y_1}(0^+, z_2, \mathbf{x}') \right) = \mathbf{w}^1(0^+, z_2, \mathbf{x}'), \\ \lim_{z_1 \rightarrow +\infty} \boldsymbol{\tau}^0(\mathbf{z}, \mathbf{x}') = \boldsymbol{\pi}^0(0^+, z_2, \mathbf{x}'), & \lim_{z_1 \rightarrow +\infty} \left(\boldsymbol{\tau}^1(\mathbf{z}, \mathbf{x}') - z_1 \frac{\partial \boldsymbol{\pi}^0}{\partial y_1}(0^+, z_2, \mathbf{x}') \right) = \boldsymbol{\pi}^1(0^+, z_2, \mathbf{x}'). \end{cases} \quad (41)$$

In the intermediate region, and with the differential operator in (32), we shall use that the equilibrium (e) in (33) applies. Also, we shall use that from (2), the constitutive relations read

$$\begin{cases} \text{(c)} & \boldsymbol{\sigma} = \frac{1}{\eta^2} (2\mu_a \boldsymbol{\varepsilon}^z + \lambda_a \text{tr}(\boldsymbol{\varepsilon}^z) I) + (2\mu_a \boldsymbol{\varepsilon}^{\mathbf{x}'} + \lambda_a \text{tr}(\boldsymbol{\varepsilon}^{\mathbf{x}'})) I, \\ \text{(c')} & \boldsymbol{\varepsilon}^{\mathbf{x}'} + \frac{1}{\eta^2} \boldsymbol{\varepsilon}^z = \frac{(1 + \nu_a)}{E_a} \boldsymbol{\sigma} - \frac{\nu_a}{E_a} \text{tr}(\boldsymbol{\sigma}) I. \end{cases} \quad (42)$$

($\boldsymbol{\varepsilon}$ stands for $\boldsymbol{\varepsilon}(\mathbf{u})$) which apply in the substrate, a=s, and in the plate, a=p. We have defined

$$\boldsymbol{\varepsilon}^z(\mathbf{u}) = \frac{1}{2} \begin{pmatrix} 2\partial_{z_1}u_1 & (\partial_{z_2}u_1 + \partial_{z_1}u_2) & \partial_{z_1}u_3 \\ (\partial_{z_2}u_1 + \partial_{z_1}u_2) & 2\partial_{z_2}u_2 & \partial_{z_2}u_3 \\ \partial_{z_1}u_3 & \partial_{z_2}u_3 & 0 \end{pmatrix}. \quad (43)$$

The continuity of the displacement is easily deduced. From (c')⁻² in (42) along with (43), v_3^0 does not depend on \mathbf{z} , and (v_1^0, v_2^0) correspond to a rigid body motion, *i.e.* $v_1^0 = \Omega_a^0(\mathbf{x}')z_2 + V_{1a}^0(\mathbf{x}')$ and $v_2^0 = -\Omega_a^0(\mathbf{x}')z_1 + V_{2a}^0(\mathbf{x}')$. The periodic boundary conditions in the substrate impose $\Omega_s^0 = 0$; next, the continuity of the displacement at $z_1 = 0$ imposes $\Omega_p^0 = \Omega_a^0 = 0$ and $\mathbf{v}^0 = \mathbf{V}^0(\mathbf{x}') = \mathbf{V}_a^0(\mathbf{x}')$. Eventually, the matching conditions (40)-(41) at order 0 impose that $\mathbf{u}^0(0^-, \mathbf{x}') = \mathbf{V}^0(\mathbf{x}') = \mathbf{w}^0(0^+, z_2, \mathbf{x}')$, and making use of (17)

$$u_1^0(0^-, \mathbf{x}') = W_1^0(\mathbf{x}'), \quad u_2^0(0^-, \mathbf{x}') = W_2^0(0^+, \mathbf{x}'). \quad (44)$$

For the same reasons, $\mathbf{v}^1 = \mathbf{V}^1(\mathbf{x}')$ is a constant displacement, which from the matching conditions (40)-(41) at the order 1 lead to the relations $\mathbf{V}^1(\mathbf{x}') = \mathbf{u}^1(0^-, \mathbf{x}')$ and

$$\mathbf{w}^1(0^+, z_2, \mathbf{x}') - \mathbf{V}^1(\mathbf{x}') = \lim_{z_1 \rightarrow +\infty} z_1 \frac{\partial \mathbf{w}^0}{\partial y_1}(0^+, z_2, \mathbf{x}'). \quad (45)$$

As the left hand side of the above relation does not depend on z_1 , we deduce that $\mathbf{V}^1(\mathbf{x}') = \mathbf{u}^1(0^-, \mathbf{x}') = \mathbf{w}^1(0^+, z_2, \mathbf{x}')$ and $\partial_{y_1} \mathbf{w}^0(0^+, z_2, \mathbf{x}') = \mathbf{0}$. From (17), we already know that $\partial_{y_1} w_1^0 = \partial_{y_1} w_3^0 = 0$ but the condition for $w_2^0 = W_2^0(y_1, \mathbf{x}')$ is not obvious and it provides the boundary condition for W_2^0 of the form

$$\frac{\partial W_2^0}{\partial y_1}(0^+, \mathbf{x}') = 0. \quad (46)$$

We now turn to the effective conditions on the force. From (e)⁻² in (33), we have $\text{div}_z \boldsymbol{\tau}^0 = \mathbf{0}$ that we integrate over $Z = \{z_1 \in (0, z_m), z_2 \in Y\} \cup \{z_1 \in (-z_m, 0), z_2 \in (-\hat{\ell}/2, \hat{\ell}/2)\}$. Accounting for i) $\boldsymbol{\tau}^0 \cdot \mathbf{n}$ continuous at $z_1 = 0$, ii) $\boldsymbol{\tau}^0 \cdot \mathbf{n} = \mathbf{0}$ between the plates and the air, iii) $\boldsymbol{\tau}^0$ periodic at $z_2 = \pm \hat{\ell}/2$ in the substrate, we get that $\int_{-\hat{\ell}/2}^{\hat{\ell}/2} \tau_{1i}^0(-z_m, z_2, \mathbf{x}') dz_2 = \int_Y \tau_{1i}^0(z_m, z_2, \mathbf{x}') dz_2$. Considering the limit $z_m \rightarrow +\infty$ and the matching conditions (40) - (41) along with $\overline{\pi_{1i}^0} = 0$ from (16), we get

$$\sigma_{1i}^0(0^-, \mathbf{x}') = 0, \quad i = 1, 2, 3, \quad (47)$$

which tells us that the plates do not couple to the substrate at the dominant order. The coupling appears at the next order, starting with $\text{div}_z \boldsymbol{\tau}^1 = \mathbf{0}$ from (e)⁻¹ in (33). As for $\boldsymbol{\tau}^0$ and using again that $\overline{\pi_{1i}^0} = 0$, we get that $\sigma_{1i}^1(0^-, \mathbf{x}') = \overline{\pi_{1i}^1}(0^+, \mathbf{x}')$; eventually, using $\overline{\pi_{1i}^1}$ in (19), we get

$$\begin{cases} \sigma_{11}^1(0^-, \mathbf{x}') = \rho_p \omega^2 \varphi \hat{h} W_1^0(\mathbf{x}'), & \sigma_{12}^1(0^-, \mathbf{x}') = -\frac{E_p}{(1 - \nu_p^2)} \frac{\varphi^3 \hat{\ell}^2}{12} \frac{\partial^3 W_2^0}{\partial y_1^3}(0^+, \mathbf{x}'), \\ \sigma_{13}^1(0^-, \mathbf{x}') = \varphi \hat{h} \left(E_p \frac{\partial^2 W_3^0}{\partial x_3^2}(\mathbf{x}') + \rho_p \omega^2 W_3^0(\mathbf{x}') \right). \end{cases} \quad (48)$$

112 *3.4. The final problem*

113 The effective problem (3) is obtained for $(\mathbf{u} = \mathbf{u}^0, \boldsymbol{\sigma} = \boldsymbol{\sigma}^0 + \eta\boldsymbol{\sigma}^1)$ in the substrate for $x_1 < 0$
 114 and $(\mathbf{u} = \mathbf{W}^0, \boldsymbol{\sigma} = \boldsymbol{\pi}^0 + \eta\boldsymbol{\pi}^1)$ in the region of the array for $x_1 > 0$. Remembering that $y_1 = x_1/\eta$
 115 and $\hat{h} = h/\eta$, $\hat{\ell} = \ell/\eta^2$, it is easy to see that (i) the Euler-Bernoulli equation in (3) is obtained
 116 from (20), (ii) the effective boundary conditions announced in (5) from (36), (38), (44), (46) and
 117 (47)-(B.35).

118 **4. Numerical validation of the effective problem for a two-dimensional problem**

119 In this section, we inspect the validity of the effective problem in a two-dimensional setting
 120 for in-plane elastic waves ($u_3 = 0, \partial_{x_3} = 0$). We solve numerically the actual problem of an
 121 incident plane wave coming from $x_1 \rightarrow -\infty$ at oblique incidence on the free surface supporting
 122 the array of plates, and Lamb waves are excited in the plates. This is done using a multimodal
 123 method with pseudo-periodic solutions in the soil and Lamb modes in the plates; the method is
 124 detailed in [55]. In the effective problem, the solution is explicit, from (3) - (5) or equivalently
 125 (6)-(7).

126 We set the material properties for the elastic substrate: $\nu_s = 0.2, E_s = 2$ GPa, $\rho_s = 1000$
 127 Kg.m^{-3} , and for the plates : $\nu_p = 0.3, E_p = 2$ GPa, $\rho_p = 500$ Kg.m^{-3} . We choose $\ell = 1$ m,
 128 $\varphi = 0.5$, and we set $\eta = \sqrt{k_T \ell} = 0.37$ ($\omega = 124$ rad.s^{-1}), hence $\kappa = 0.64$ m^{-1} . We shall
 129 consider $h \in (0, 30)$ m resulting in $\kappa h \in (0, 20)$ which includes the first 6 bending modes for
 130 $h = h_n, n = 1, \dots, 6$: $h_1 \simeq 3$ m, $h_2 \simeq 7.3$ m, $h_3 \simeq 12.3$ m, $h_4 = 17.2$ m, $h_5 = 22.1$ m,
 131 $h_6 = 27.0$ m. The first resonance of the quasi-longitudinal wave along x_1 appears for $h =$
 132 $\pi/(2\omega) \sqrt{E_p/((1 - \nu_p^2)\rho_p)} \simeq 26.5$ m, hence it will be visible in our results.

133 *4.1. Reflection of elastic waves - the solution of the effective problem*

We define the potentials (ϕ, ψ) using the Helmholtz decomposition, with $\mathbf{u} = \nabla\phi + \nabla \times (\psi \mathbf{e}_3)$.
 The incident wave in the substrate is defined in terms of the incident potentials

$$\begin{cases} \phi^{\text{inc}}(x_1, x_2) = A_L e^{i\alpha_L x_1} e^{i\beta x_2}, & \psi^{\text{inc}}(x_1, x_2) = A_T e^{i\alpha_T x_1} e^{i\beta x_2}, \\ \text{with } (\alpha_L, \beta) = k_L (\cos \theta_L, \sin \theta_L), & (\alpha_T, \beta) = k_T (\cos \theta_T, \sin \theta_T), \end{cases} \quad (49)$$

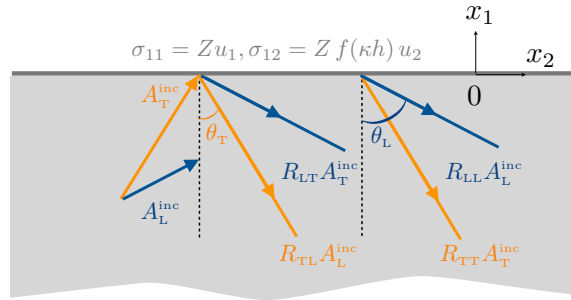


Figure 5: The effective (partial) problem – Reflection of an elastic wave on the surface $x_1 = 0$ where effective boundary conditions (6) apply. The incident wave is defined by (49) and the solution by (50). The arrows show the wavevectors.

with $k_L = \sqrt{\frac{\rho_s}{\lambda_s + 2\mu_s}} \omega$ and $k_T = \sqrt{\frac{\rho_s}{\mu_s}} \omega$. The solution in the substrate reads

$$\begin{cases} \phi(x_1, x_2) = \phi^{\text{inc}}(x_1, x_2) + (R_{LL} A_L + R_{LT} A_T) e^{-i\alpha_L x_1} e^{i\beta x_2}, \\ \psi(x_1, x_2) = \psi^{\text{inc}}(x_1, x_2) + (R_{TL} A_L + R_{TT} A_T) e^{-i\alpha_T x_1} e^{i\beta x_2}. \end{cases} \quad (50)$$

The effective problem can be solved explicitly. Accounting for the boundary conditions (6), it is easy to show that

$$\begin{cases} R_{LL} = \frac{1}{D} \left[\sin 2\theta_T \sin 2\theta_L - \xi^2 \cos^2 2\theta_T - i\xi a (\cos \theta_L - \xi f \cos \theta_T) - \xi a^2 f \cos(\theta_L + \theta_T) \right], \\ R_{TT} = \frac{1}{D} \left[\sin 2\theta_T \sin 2\theta_L - \xi^2 \cos^2 2\theta_T + i\xi a (\cos \theta_L - \xi f \cos \theta_T) - \xi a^2 f \cos(\theta_L + \theta_T) \right], \\ R_{LT} = -\frac{\xi^2 \sin 2\theta_T}{D} (2 \cos 2\theta_T + a^2 f), \quad R_{TL} = \frac{\sin 2\theta_L}{D} (2 \cos 2\theta_T + a^2 f), \\ \text{where } D = \sin 2\theta_T \sin 2\theta_L + \xi^2 \cos^2 2\theta_T - i\xi a (\cos \theta_L + \xi f \cos \theta_T) - \xi a^2 f \cos(\theta_L - \theta_T), \\ f \text{ stands for } f(\kappa h) \text{ in (7) and } \xi = \frac{\sin \theta_L}{\sin \theta_T} = \sqrt{\frac{2(1 - \nu_s)}{1 - 2\nu_s}}, \quad a = \varphi \frac{\rho_p}{\rho_s} k_T h. \end{cases} \quad (51)$$

134 In the above expressions $a = Z/(\mu_s k_T)$ (and Z in (7)) measures the strength of the coupling
135 between the plates and the substrate. Expectedly for $a = 0$ in (51), we recover the reflection
136 coefficients for a flat interface, see *e.g.* [56]. It is worth noting that the same reflection coefficients
137 are obtained by solving the complete problem (3)-(5).

138 As previously done, the displacement fields in the region of the plates $x_1 \in (0, h)$ are ob-
139 tained owing to the linearity of $u_i(x_1, x_2)$ with respect to $u_i(0, x_2)$, $i = 1, 2$, and the continuity of
140 $u_i(0, x_2)$ between the plates and the substrate, see Appendix A. The displacements $u_i(0, x_2)$ can
141 be calculated from the reflection coefficients in (51), resulting in

$$\begin{aligned} u_1(x_1, x_2) &= u_1(0, x_2), \quad u_2(x_1, x_2) = u_2(0, x_2)V(x_1), \\ \begin{cases} u_1(0, x_2) = \frac{i\xi^2 k_L}{D} [2 \cos \theta_L (\cos 2\theta_T - i \cos \theta_T a f) A_L + \sin 2\theta_T (2 \cos \theta_L - i\xi a f) A_T] e^{i\beta x_2}, \\ u_2(0, x_2) = \frac{ik_T}{D} [\sin 2\theta_L (2 \cos \theta_T - ia) A_L - 2\xi \cos \theta_T (\xi \cos 2\theta_T - ia \cos \theta_L) A_T] e^{i\beta x_2}, \\ V(x_1) = \frac{V_1(\kappa h) [\text{ch}\kappa(x_1 - h) + \cos \kappa(x_1 - h)] + V_2(\kappa h) [\text{sh}\kappa(x_1 - h) + \sin \kappa(x_1 - h)]}{2(1 + \text{ch}\kappa h \cos \kappa h)}, \\ \text{with } V_1(\kappa h) = (\text{ch}\kappa h + \cos \kappa h), \quad V_2(\kappa h) = (\text{sh}\kappa h - \sin \kappa h). \end{cases} \end{cases} \quad (52)$$

142 As a reference case, typical displacement fields (u_1, u_2) for a surface on its own ($h = 0$) are
143 reported in figure 6 for three incident angles θ_L . The incident wave is of the form (49) with
144 $A_L = 1/(2\beta)$, $A_T = -1/(2\alpha_T)$ producing an incident horizontal displacement equal to one meter at
145 $x_1 = 0$.

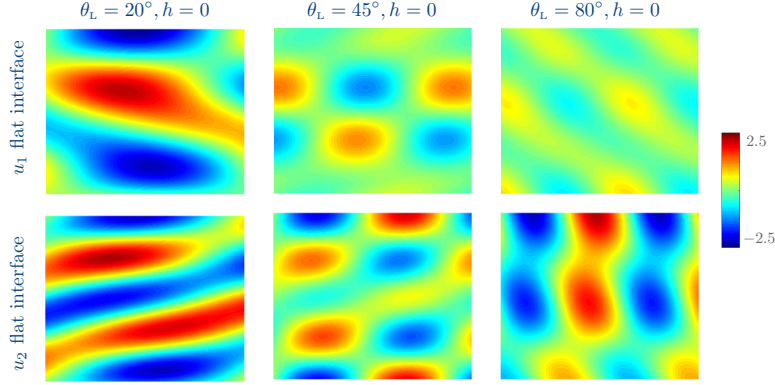


Figure 6: Reference case – Vertical u_1 and horizontal u_2 displacement fields inside the substrate in the absence of array of plates (linear colorscale in m) for three different angles θ_L . The fields are shown for $x_1 \in (-100, 0)$ m and $x_2 \in (0, 120)$ m.

146 4.2. Weak and strong interactions between plates and substrate

147 The effect of the array of plates is encapsulated in the impedance parameters (a, f), or equiv-
 148 alently ($Z = \mu_s k_T a, f$), whose variations versus $k_T h$ are reported in figure 7. The parameter
 149 $Z = \rho_p \omega^2 \varphi h$ tells us that heavier plates and higher frequencies produce higher coupling with
 150 the substrate, which is not surprising. The parameter f encapsulates the effects of the bending
 151 resonances and it diverges when approaching them. This occurs at the frequencies such that
 152 $\text{ch} \kappa h \cos \kappa h = -1$ which correspond to a clamped- free single plate ($u_2(0, x_2) = 0$ from (6) im-
 posed by $Z \rightarrow \infty$).

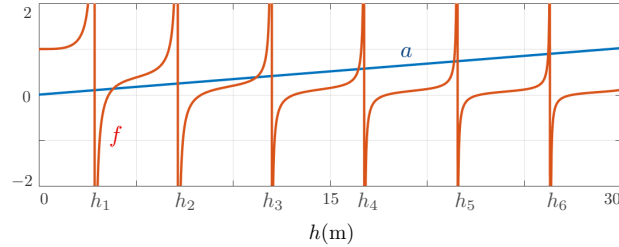


Figure 7: Variations of the impedance parameters $a = Z/(\mu_s k_T)$ in (51), and f in (7), versus h . The parameter f diverges at the resonances of the clamped - free plates for $\text{ch} \kappa h \cos \kappa h = -1$.

153

154 4.2.1. Weak interaction

155 Between two successive resonances, the interaction between the substrate and the plates is
 156 weak. Indeed, from (6), with Z being small and $f(\kappa h)$ of the order of unity, the wave impinging
 157 the surface sees essentially a flat surface, with $\sigma_{11} \simeq \sigma_{12} \simeq 0$ at $x_1 = 0$. The resulting patterns,
 158 not reported, are indeed similar to those obtained for $h = 0$ in figure 6. Since there is not much
 159 to be said on the field in the substrate, we focus on the capability of the complete effective
 160 solution to reproduce the actual displacement in the plates. Figures 8 show a small region of
 161 the displacement fields near the interface ($\theta_L = 45^\circ$ and $h = 5$ m resulting in $k_T h = 0.7$).

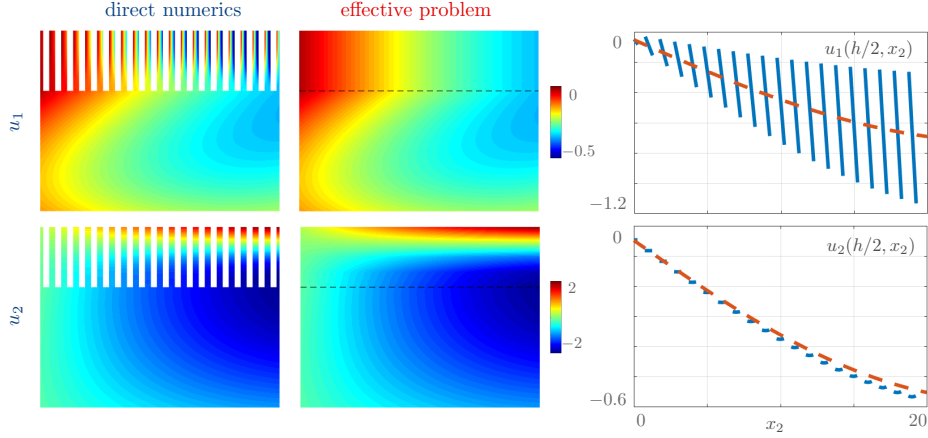


Figure 8: Meaning of the homogenization process – Displacement fields (actual and homogenized) for $x_1 \in (-10, 5)$ m and $x_2 \in (0, 20)$ m ($h = 5$ m, $\theta_L = 45^\circ$).

162 From what we have said (the interaction is weak), the displacements in the substrate are neatly
 163 reproduced. More interestingly, the displacements in the plates are also accurately reproduced
 164 in an "averaged" sense which clearly appears for the displacement u_1 : in the actual problem, u_1
 165 varies linearly with x_2 within a single plate, in agreement with (21); this variation at the small
 166 scale is superimposed to a variation, at large scale, from one plate to the other. The small scale
 167 variations do not appear in the homogenized solution; it is the scale which aims to disappear in
 168 the homogenization procedure. It remains that the large scale variations are neatly captured. The
 169 same occurs for u_2 but in this case, the small scale variations are less visible because they appear
 170 at the order 2 (see (17) and (27)).

171 4.2.2. Strong coupling near the resonances

172 Strong coupling in the vicinity of the bending resonances can be measured by the amplitudes
 of the displacements in the plates. We report in figure 9 the amplitudes of the horizontal displacements

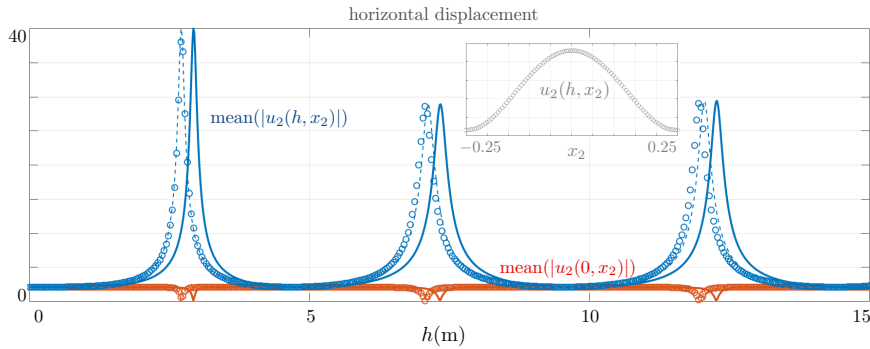


Figure 9: Amplitude of u_2 at $x_1 = 0$ and $x_1 = h$ against h , from direct numerics (symbols) and from the effective solution (52) (plain line); $\theta_L = 45^\circ$. Shifts in the resonances $h \rightarrow h - h_0$, with $h_0 = 0.22$ m are compensated (dashed line). The inset shows the actual variation of $u_2(h, x_2)$ within a single plate with variations as small as about 10^{-4} with respect to the mean value.

173 ment u_2 against h , at the bottom and at the top of a single plate. In the actual problem these am-
 174 plitudes are calculated by averaging over $x_2 \in (-\ell_p/2, \ell_p/2)$ the profiles $|u_2(0, x_2)|$ and $|u_2(h, x_2)|$
 175 obtained numerically. In the homogenized problem $|u_2(0, x_2)|$ and $|u_2(h, x_2)| = |V(h)u_2(0, x_2)|$ are
 176 given in closed-forms from (52).

For $h \in (0, 15)$ m, the first three bending resonances are visible by means of high displacements at the top of the plates (up to 40 times the amplitude of the incident wave in the reported case). It is also visible by means of vanishing amplitude at the bottom of the plate, in agreement with (52) for $f \rightarrow \infty$. Hence, near the bending resonances, the plates, with clamped-free boundary conditions, impose a vanishing horizontal displacement at the interface with the substrate, a fact already mentioned in [22]. In the substrate, the resulting displacements are significantly impacted. Large values of $f(\kappa h)$ produce

$$R_{LL} \simeq -1 - 2ia \frac{\cos \theta_L}{\xi}, \quad R_{TT} \simeq 1 + 2ia \frac{\sin^2 \theta_T}{\cos \theta_T}, \quad R_{TL} \simeq 2ia \frac{\sin \theta_T \cos \theta_L}{\xi \cos \theta_T}, \quad R_{LT} \simeq -2ia \sin \theta_T. \quad (53)$$

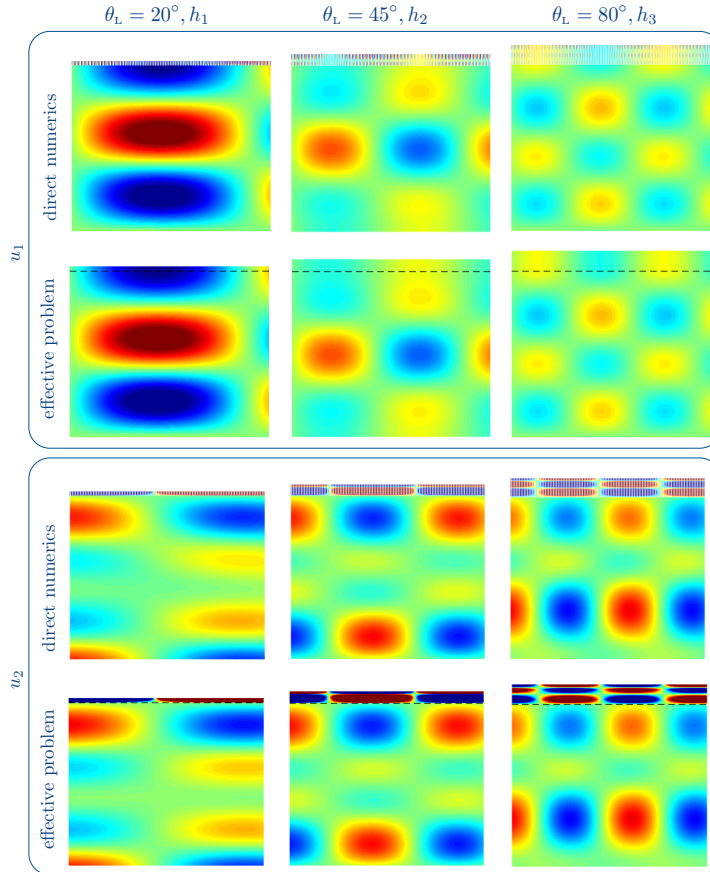


Figure 10: Strong coupling between the substrate and the array of plates near the three first bending resonances – The values of h_n , $n = 1, 2, 3$ have been taken from figure 9 at the maximum displacements in the direct numerics and in the homogenized solution ($h_1 \simeq 3$ m, $h_2 \simeq 7.3$ m, $h_3 \simeq 12.3$ m). Same representation as in figure 6.

from (51), hence

$$\begin{cases} u_1(x_1, x_2) \approx 2ik_L (A_L \cos \theta_L \cos \alpha_L x_1 + A_T \sin \theta_L \cos \alpha_T x_1) e^{i\beta x_2} + O(a), \\ u_2(x_1, x_2) \approx -2k_T (A_L \sin \theta_L \sin \alpha_L x_1 - A_T \cos \theta_T \sin \alpha_T x_1) e^{i\beta x_2} + O(a), \end{cases} \quad (54)$$

177 corresponding essentially to a superposition of standing waves. Examples of resulting patterns
 178 are shown in figure 10 for the first three bending resonances to be compared with those obtained
 179 for a flat interface in figure 6. It is worth noting that in figure 10 we have accounted for the shift
 180 in h_n , $n = 1, 2, 3$ in the homogenized solution from figure 9 ($h_1 \approx 3$ m, $h_2 \approx 7.3$ m, $h_3 \approx 12.3$
 181 m), where a systematic shift of the effective solution $h \rightarrow h - h_0$, with $h_0 = 0.22$ m in the present
 182 case.

183 4.3. Occurrence of the first longitudinal resonance

184 To go further in the analysis, we report in figure 11 the reflection coefficients against $h \in$
 185 $(0, 25)$ m and $\theta \in (0, 90^\circ)$. We represent the real and imaginary parts of the 4 reflection coeffi-
 186 cients. As previously said, our analysis does not hold at and above the first longitudinal reso-

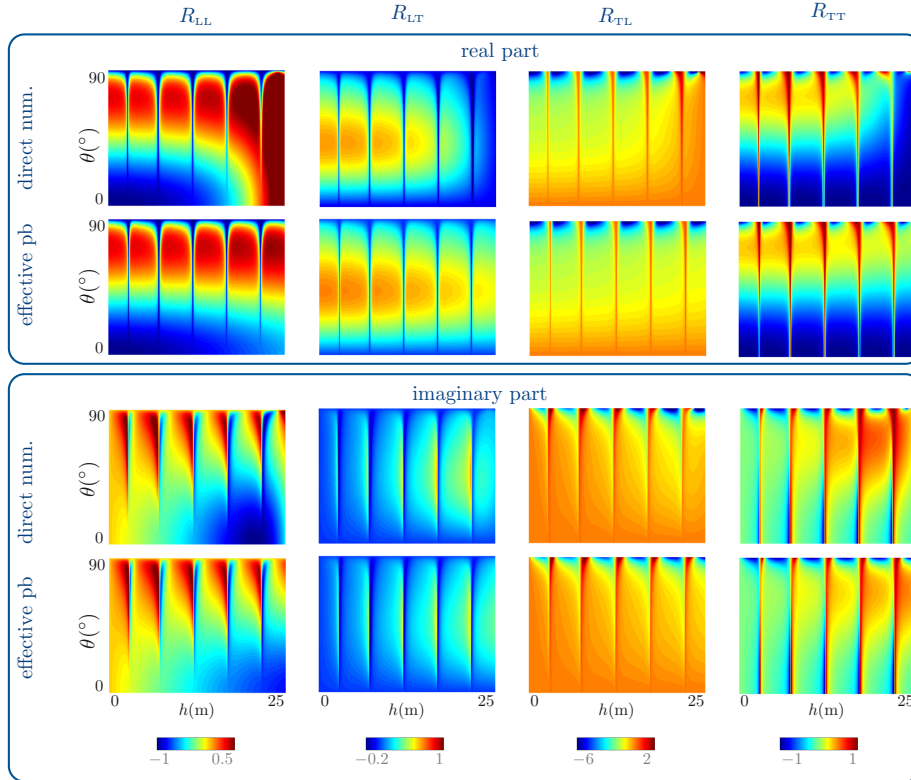


Figure 11: Accuracy of the effective model on the reflection coefficients – Real and imaginary parts of the reflection coefficients versus h and θ . The effective coefficients (51) (second row) reproduce accurately the actual ones (first row) up to the first longitudinal resonance for $h \approx 26.5$ m.

187 nance, which appears for $h \simeq 26.5$ m; expectedly, the effective model indeed breaks down when
 188 approaching this high value but it remains surprisingly accurate up to $h \sim 15$ m (hence $k_T h \sim 2$).

189 The occurrence of this resonance is visible by means of the amplitude of the vertical displacement
 190 $u_1(0, x_2)$, which is reported in figure 12 against h . We observe the same trends as for the
 191 bending modes. Far from the resonance, the displacement is essentially the same as for a surface
 192 on its own; at the longitudinal resonance, it tends to zero resulting in clamped- free conditions
 193 for the plates. However, it is also visible that rapid variations of the displacements due to multiple
 194 bending resonances superimpose to the smooth variations of the displacement due to the
 195 longitudinal resonance.

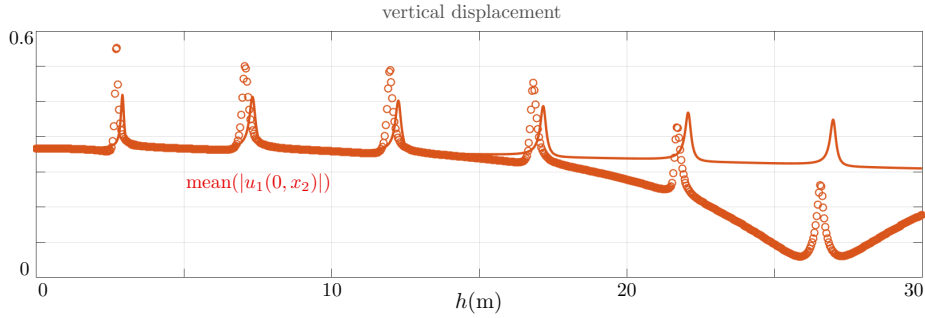


Figure 12: Occurrence of the first resonance in reflection – Variation of the amplitude of the vertical displacement $u_1(0, x_2)$ at the bottom of the plates. The bending resonances are superimposed to the longitudinal resonance which produces an almost clamped condition $u_1(0, x_2) = 0$ for $h \simeq 26.5$ m.

196 4.4. Comment on a mass-spring model used in [22]

As previously said, impedance conditions implying a simple mass-spring resonator have been used previously in the literature. It was pointed out in [22] that “for practical applications, these simple cases can be extended to more complex cases, for instance slender beam or plate resonators”, and this is the subject of the present study. For the sake of completeness, we report here the results from [22] in the case of mass-spring resonators forming an “isotropic horizontally resonant surface” as a simplified version of an array of beams with flexural resonances. In the absence of damping and adapting the notations, the reflection coefficients given in §4 of [22] (see after (12)) read

$$\left\{ \begin{array}{l} R_{LL}^{m-s} = \frac{1}{D^{m-s}} \left[\sin 2\theta_T \sin 2\theta_L - \xi^2 \cos^2 2\theta_T + i\xi^2 a f^{m-s} \cos \theta_T \right], \\ R_{TT}^{m-s} = \frac{1}{D^{m-s}} \left[\sin 2\theta_T \sin 2\theta_L - \xi^2 \cos^2 2\theta_T - i\xi^2 a f^{m-s} \cos \theta_T \right], \\ R_{LT}^{m-s} = -\frac{\xi^2 \sin 2\theta_T}{D^{m-s}} 2 \cos 2\theta_T, \quad R_{TL}^{m-s} = \frac{\sin 2\theta_L}{D^{m-s}} 2 \cos 2\theta_T, \\ \text{where } D^{m-s} = \sin 2\theta_T \sin 2\theta_L + \xi^2 \cos^2 2\theta_T - i\xi^2 a f^{m-s} \cos \theta_T, \quad f^{m-s} = \left(1 - \left(\frac{\omega}{\omega_{res}} \right)^2 \right)^{-1}, \end{array} \right. \quad (55)$$

197 where m-s stands for mass-spring and ω_{res} is one resonance frequency. There are two noticeable
 198 differences between (55) and (51). The most obvious is that f is approximated locally with

199 f^{m-s} . However the capability of f^{m-s} to reproduce the variation of f is limited; besides a simple
 200 summation of f^{m-s} for the succession of resonances is not satisfactory. Next, there are missing
 201 terms in the reflection coefficients. This is attributable to the implicit assumption $\sigma_{11} = 0$ far
 202 from the longitudinal resonance (instead of our expression in (5)) which is not true for real
 203 plate/beam resonators. The consequence is illustrated in figure 13 where we report the reflection
 204 coefficient R_{LL} against h from our model (51) and from [22] (55) together with the numerical
 result. Expectedly, the mass-spring model reasonably captures the physics of the interaction but

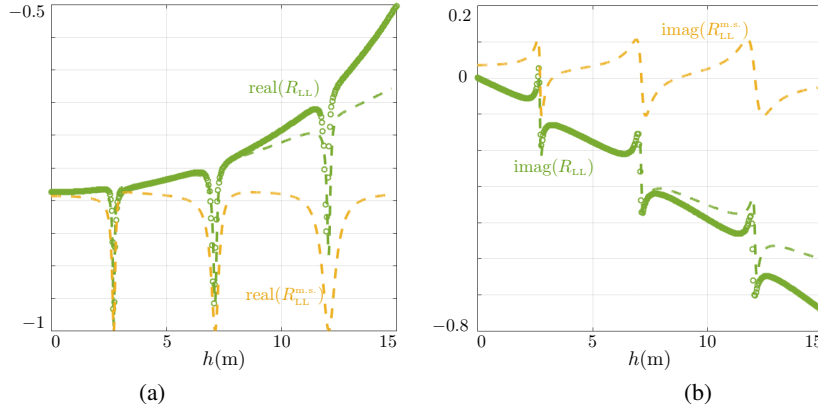


Figure 13: Reflection coefficient against h for $\theta_L = 20^\circ$ – R_{LL} (green dashed lines) from (51) and R_{LL}^{m-s} (yellow dashed lines) from (55) for mass-spring resonators considered in [22]; (a) real part and (b) imaginary part. The results from direct numerics are shown in symbols (the same shift $h \rightarrow h - h_0$, with $h_0 = 0.22$ m as in figure 9 have been used for readability).

205 it clearly fails in a quantitative prediction. On the one hand the sharpnesses of the successive
 206 resonances is not reproduced. More visible is the fact that the slow variation of R_{LL} with h
 207 is missed; notably, the reflexion at flexural resonances significantly departs from the simple
 208 prediction $R_{LL} = -1$ given by (55), see (53)¹.
 209

210 5. Conclusion

211 We have studied the interaction of an array of plates or beams with an elastic half-space using
 212 asymptotic analysis and homogenization techniques. The resulting models (3)-(5) for plates
 213 and (B.1)-(B.3) for beams provide one-dimensional propagation problems which in their simpler
 214 form consist in effective boundary conditions at the surface of the ground, (6) for plates and (B.5)
 215 for beams. The exception for plates in the boundary condition σ_{13} in (5) is incidental for in-plane
 216 incidence but it is interesting since it provides non trivial coupling for arbitrary incidence. For
 217 in-plane incidence, the model has been validated by comparison with direct numerical simula-
 218 tions thanks to the multimodal method which show an overall good agreement. In particular,

¹It is worth noting that this discrepancy is attributable to the contribution of the longitudinal motions; it does not impact the condition of vanishing horizontal velocity at the free surface. Specifically, in (54), we have

$$u_2(x_1, x_2) = -2k_T (A_L \sin \theta_L \sin \alpha_L x_1 - A_T \cos \theta_T \sin \alpha_T x_1) e^{i\beta x_2} - k_T \alpha \frac{\sin 2\theta_T}{\xi \cos \theta_T} (\cos \theta_L A_L + \sin \theta_L A_T) (e^{-i\alpha_L x_1} - e^{-i\alpha_T x_1}),$$

hence $u_2(0, x_2) = 0$ as imposed by (6) when $f \rightarrow \infty$.

219 the displacement fields obtained in a closed-form accurately reproduce the actual ones; this is
 220 of practical importance for applications to site-city interaction where the displacements at the
 221 bottom and at the top of buildings are relevant quantities to measure the risk of building damage.

222 Our models have been obtained owing to a deductive approach which can be applied to a
 223 wide variety of problems. An important point is that the analysis does not assume a preliminary
 224 model reduction for the resonator on its own and as such, it can be conducted at any order. Higher
 225 order models would involve enriched transmission and boundary conditions able to capture more
 226 subtle effects as the shift in the resonance frequencies visible in the figure 9 or the presence
 227 of heterogeneity at the roots and at the top of the bodies as it has been done in [37]. Next,
 228 we have considered bodies with sufficient symmetry resulting in a diagonal rigidity matrices
 229 and which greatly simplify calculations. When symmetries are lost, and the simplest case is
 230 that of beams with rectangular cross-sections, the calculations are similar; they will produce
 231 couplings for incidences as soon as the horizontal component does not coincide with one of
 232 the two principal directions. Additional complexities can be accounted for straightforwardly, as
 233 orthotropic anisotropy along x_1 or slow variations in the cross-section. Eventually, the models
 234 are restricted to the low frequency regime where only the flexural resonances take place. At the
 235 onset of the first longitudinal resonance, they fail as illustrated in figure 12. Extension of the
 236 present work consists in adapting the present homogenization procedure in order to capture both
 237 flexural and longitudinal resonances and their interplay at higher frequencies.

238 Acknowledgements

239 K.P. acknowledges support of the ANR (contract number ANR-19-CE08-0006). A.M. and
 240 S.G. acknowledge insightful discussions with Philippe Roux at the Institute ISTerre of the Uni-
 241 versity of Grenoble-Alpes. S.G. is also thankful for a visiting position in the group of Richard
 242 Craster within the Department of Mathematics at Imperial College London in 2018-2019.

243 Appendix A. Remark on the solution in the region of the plates

From the boundary conditions (5), $\frac{\partial^2 u_2}{\partial x_1^2}(h, x_2) = \frac{\partial^3 u_2}{\partial x_1^3}(h, x_2) = 0$ and $u_2(0^+, x_2) = u_2(0^-, x_2)$,
 $\frac{\partial u_2}{\partial x_1}(0^+, x_2) = 0$, the general solution for $x_1 \in (0, h)$ reads as follows

$$\begin{cases} u_2(x_1, x_2) = A(x_2) \{a(\kappa h) [\text{ch}\kappa(x_1 - h) + \cos \kappa(x_1 - h)] + b(\kappa h) [\text{sh}\kappa(x_1 - h) + \sin \kappa(x_1 - h)]\}, \\ \text{with } a(\kappa h) = (\text{ch}\kappa h + \cos \kappa h), \quad b(\kappa h) = (\text{sh}\kappa h - \sin \kappa h). \end{cases} \quad (\text{A.1})$$

The displacement u_2 is continuous at $x_1 = 0$ and we have $2A(x_2)(1 + \text{ch}\kappa h \cos \kappa h) = u_2(0, x_2)$,
 hence

$$\begin{cases} u_2(x_1, x_2) = u_2(0, x_2)V(x_1), \\ V(x_1) = \frac{a(\kappa h) [\text{ch}\kappa(x_1 - h) + \cos \kappa(x_1 - h)] + b(\kappa h) [\text{sh}\kappa(x_1 - h) + \sin \kappa(x_1 - h)]}{2(1 + \text{ch}\kappa h \cos \kappa h)}. \end{cases} \quad (\text{A.2})$$

244 Obviously, this holds except at the resonance frequencies of the plates for $\text{ch}\kappa h \cos \kappa h = -1$
 245 which imposes $u_2(0, x_2) = 0$ (and eigenmodes in the region of the plates). It follows that the

246 relation on $\sigma_{12}(0^-, \mathbf{x}')$ in (5) becomes $\sigma_{12}(0^-, \mathbf{x}') = -(D_p/\ell)V''''(0) u_2(0, x_2)$, with $V''''(0) =$
 247 $-\kappa^4 h f(\kappa h)$, with $f(\kappa h)$ in (6). With $\sigma_{12}(0^-, \mathbf{x}') = (\kappa^4 D_p h/\ell)f(\kappa h) u_2(0, x_2)$ and $\kappa^4 D_p = \rho_p \omega^2 \varphi \ell$,
 we recover the form announced in (6).

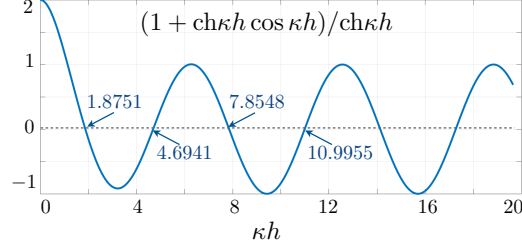


Figure A.14: Bending resonances in the region of the plates (clamped/stress free conditions).

248

249 Appendix B. Main steps of the derivation for an array of beams of circular section

Let us derive in this Appendix the effective model for beams of circular section with radius r_p , for which all the derivations are analytical; the circular beams are periodically located in an array whose unit cell has a section area S (figure 1(b)). In this case, the complete formulation of the problem reads

$$\left\{ \begin{array}{l} \text{In the substrate, } x_1 \in (-\infty, 0) : \quad \operatorname{div} \boldsymbol{\sigma} + \rho_s \omega^2 \mathbf{u} = \mathbf{0}, \quad \boldsymbol{\sigma} = 2\mu_s \boldsymbol{\varepsilon} + \lambda_s \operatorname{tr}(\boldsymbol{\varepsilon}) I, \\ \text{In the region of the beams, } x_1 \in (0, h) : \quad \frac{\partial^4 u_\alpha}{\partial x_1^4} - \kappa^4 u_\alpha = 0, \quad \alpha = 2, 3, \quad \kappa = \left(\frac{\rho_p \omega^2 \pi r_p^2}{D_p} \right)^{1/4}, \end{array} \right. \quad (\text{B.1})$$

where

$$D_p = E_p \frac{\pi r_p^4}{4}, \quad (\text{B.2})$$

is the flexural rigidity of the beams, complemented by the boundary conditions

$$\left\{ \begin{array}{l} \sigma_{11}(0^-, \mathbf{x}') = \rho_p \omega^2 \varphi h u_1(0, x_2), \\ \sigma_{1\alpha}(0^-, \mathbf{x}') = -\frac{D_p}{S} \frac{\partial^3 u_\alpha}{\partial x_1^3}(0^+, x_2), \\ u_\alpha(0^+, \mathbf{x}') = u_\alpha(0^-, \mathbf{x}'), \quad \frac{\partial u_\alpha}{\partial x_1}(0^+, \mathbf{x}') = 0, \\ \frac{\partial^2 u_\alpha}{\partial x_1^2}(h, \mathbf{x}') = \frac{\partial^3 u_\alpha}{\partial x_1^3}(h, \mathbf{x}') = 0, \quad \alpha = 2, 3. \end{array} \right. \quad (\text{B.3})$$

where $\varphi = \pi r_p^2/S$. It follows that the problem can be thought in the substrate only, with

$$\operatorname{div} \boldsymbol{\sigma} + \rho_s \omega^2 \mathbf{u} = \mathbf{0}, \quad \boldsymbol{\sigma} = 2\mu_s \boldsymbol{\varepsilon} + \lambda_s \operatorname{tr}(\boldsymbol{\varepsilon}) I, \quad x_1 \in (-\infty, 0), \quad (\text{B.4})$$

along with the boundary conditions of the Robin's type

$$\begin{cases} \sigma_{11}(0, \mathbf{x}') = Z u_1(0, \mathbf{x}'), \\ \sigma_{1\alpha}(0, \mathbf{x}') = Z f(\kappa h) u_\alpha(0, \mathbf{x}'), \end{cases} \quad (\text{B.5})$$

250 where Z and $f(\kappa h)$ are defined in (7) (we used that $D_p \kappa^4 = \rho_p \omega^2 \pi r_p^2$).

251 *Appendix B.1. Effective wave equation in the region of the beams*

252 *Appendix B.1.1. Notations*

We shall use the same expansions as in (9) but now, the terms \mathbf{w}^n and $\boldsymbol{\pi}^n$ depend on $\mathbf{z}' = (z_2, z_3)$ (and not only on z_2) and we seek to establish the effective behaviour in the region of the array in terms of macroscopic averaged fields

$$\overline{\mathbf{w}^n}(y_1, \mathbf{x}') = \frac{1}{\varphi \hat{S}} \int_Y \mathbf{w}^n(y_1, \mathbf{z}', \mathbf{x}') d\mathbf{z}', \quad \overline{\boldsymbol{\pi}^n}(y_1, \mathbf{x}') = \frac{1}{\hat{S}} \int_Y \boldsymbol{\pi}^n(y_1, \mathbf{z}', \mathbf{x}') d\mathbf{z}', \quad (\text{B.6})$$

where $\mathbf{x}' = (x_2, x_3)$ and Y represents the circular section of the beam $Y = \left\{ \sqrt{z_2^2 + z_3^2} \leq \hat{r} \right\}$, with $\hat{r} = r_p / \eta^2$ and $\hat{S} = S / \eta^4$. It is worth noting that it is sufficient to replace z_2 by \mathbf{z}' in (10) to (15); in particular, we have

$$\nabla \rightarrow \frac{e_1}{\eta} \frac{\partial}{\partial y_1} + \frac{1}{\eta^2} \nabla_{\mathbf{z}'} + \nabla_{\mathbf{x}'}. \quad (\text{B.7})$$

and

$$\boldsymbol{\varepsilon}^{\mathbf{z}'}(\mathbf{w}) = \frac{1}{2} \begin{pmatrix} 0 & \partial_{z_2} w_1 & \partial_{z_3} w_1 \\ \partial_{z_2} w_1 & 2\partial_{z_2} w_2 & (\partial_{z_3} w_2 + \partial_{z_2} w_3) \\ \partial_{z_3} w_1 & (\partial_{z_3} w_2 + \partial_{z_2} w_3) & 2\partial_{z_3} w_3 \end{pmatrix}. \quad (\text{B.8})$$

253 *Appendix B.1.2. Sequence of resolution and main results of the analysis*

254 The analysis becomes more involved since the problem is two-dimensional in the rescaled
255 coordinate \mathbf{z}' . The procedure is thus more complex. It is as follows:

1. We establish that

$$\overline{\pi_{11}^0} = 0, \quad (\text{B.9})$$

and the dependence of \mathbf{w}^0 on (z_2, z_3) , specifically

$$w_1^0 = W_1^0(\mathbf{x}'), \quad w_\alpha^0 = W_\alpha^0(y_1, \mathbf{x}'), \quad (\text{B.10})$$

2. We deduce the form of $\boldsymbol{\pi}^0$ and of \mathbf{w}^1

$$\begin{cases} \pi_{11}^0 = -E_p \frac{\partial^2 W_\alpha^0}{\partial y_1^2}(y_1, \mathbf{x}') z_\alpha, & \pi_{1\alpha}^0 = \pi_{\alpha\beta}^0 = 0, \\ w_1^1 = W_1^1(\mathbf{x}') - \frac{\partial W_\alpha^0}{\partial y_1}(y_1, \mathbf{x}') z_\alpha, & w_\alpha^1 = W_\alpha^1(y_1, \mathbf{x}'). \end{cases} \quad (\text{B.11})$$

3. eventually the form of $\overline{\pi_{1i}^1}$ and the Euler-Bernoulli equation for the bending W_α^0 , $\alpha = 2, 3$.
Specifically

$$\begin{cases} \overline{\pi_{11}^1}(y_1, \mathbf{x}') = \rho_p \omega^2 \varphi W_1^0(\mathbf{x}') (\hat{h} - y_1), \\ \overline{\pi_{1\alpha}^1}(y_1, \mathbf{x}') = -E_p \frac{\varphi \hat{r}^2}{4} \frac{\partial^3 W_\alpha^0}{\partial y_1^3}(y_1, \mathbf{x}'), \end{cases} \quad (\text{B.12})$$

and

$$E_p \frac{\hat{r}^2}{4} \frac{\partial^4 W_\alpha^0}{\partial y_1^4} - \rho_p \omega^2 W_\alpha^0 = 0. \quad (\text{B.13})$$

256

257 *Appendix B.1.3. First step: $\overline{\pi_{11}^0}$ in (B.9) and \mathbf{w}^0 in (B.10)*

258 This step is not very demanding. From $(E_1)^{-1}$ in (13), $\partial_{y_1} \pi_{11}^0 + \partial_{z_\alpha} \pi_{1\alpha}^1 = 0$, which after
259 integration over Y leaves us with $\partial_{y_1} \overline{\pi_{11}^0} = 0$; anticipating $\overline{\pi_{11}^0} = 0$ at the top of the beams (as we
260 did for the plates), we get $\overline{\pi_{11}^0} = 0$ everywhere, as announced in (B.9).

Now, from $(C'_{1\alpha})^{-2}$ in (14), $\partial_{z_\alpha} w_1^0 = 0$ and from $(C'_{11})^{-1}$ $\partial_{y_1} w_1^0 = 0$. It follows that w_1^0 depends
only on \mathbf{x}' , in agreement with (B.10). From $(C'_{\alpha\beta})^{-2}$, w_α^0 is a rigid body motion *i.e.*

$$w_\alpha^0 = W_\alpha^0(y_1, \mathbf{x}') + \Omega^0(y_1, \mathbf{x}')(\mathbf{e}_1, \mathbf{z}', \mathbf{e}_\alpha), \quad (\text{B.14})$$

with $(\mathbf{e}_1, \mathbf{z}', \mathbf{e}_\alpha) = \mathbf{e}_1 \cdot (\mathbf{z}' \times \mathbf{e}_\alpha)$ being the triple product, and we shall establish that $\Omega^0 = 0$. To do
so we infer, from $(C'_{1\alpha})^{-1}$, that

$$\partial_{z_\alpha} w_1^1 + \partial_{y_1} w_\alpha^0 = 0, \quad \Rightarrow \quad \partial_{y_1} (\partial_{z_2} w_3^0 - \partial_{z_3} w_2^0) = 0. \quad (\text{B.15})$$

261 Inserting (B.14) in (B.15) tells us that Ω^0 does not depend on y_1 and anticipating the matching
262 condition with the displacement in the substrate which imposes that $\Omega^0 = 0$ at $y_1 = 0$ (see
263 forthcoming (B.41)), we deduce that $\Omega^0 = 0$ everywhere, and (B.14) reduces to the form of w_α^0
264 announced in (B.10).

265 *Appendix B.1.4. Second step: (π^0, \mathbf{w}^1) in (B.11)*

We start by determining \mathbf{w}^1 incompletely (compared to what is announced in (B.10)). For
 w_1^1 , we come back to $\partial_{z_\alpha} w_1^1 + \partial_{y_1} w_\alpha^0 = 0$ in (B.15), and w_α^0 in (B.10) provides us with

$$w_1^1 = W_1(y_1, \mathbf{x}') - \frac{\partial W_\alpha^0}{\partial y_1}(y_1, \mathbf{x}') z_\alpha, \quad (\text{B.16})$$

and it remains for us to show that W_1 does not depend on y_1 ; this will be done after π_{11}^0 has been
determined. Next, from $(C'_{\alpha\beta})^{-1}$, w_α^1 is a rigid body motion, hence

$$w_\alpha^1 = W_\alpha^1(y_1, \mathbf{x}') + \Omega^1(y_1, \mathbf{x}')(\mathbf{e}_1, \mathbf{z}', \mathbf{e}_\alpha). \quad (\text{B.17})$$

Now, we shall prove that $\Omega^1 = 0$; this will be done once $\pi_{1\alpha}^0$ have been determined. For the
time being, we pursue the calculations by setting the boundary value problem set in Y for the

unknowns $(\pi_{\alpha\beta}^0, w_\alpha^2)$. From $(E_\alpha)^{-2}$ and $(C_{\alpha\beta})^0$ in (13), it reads

$$\begin{cases} \partial_{z_\beta} \pi_{\alpha\beta}^0 = 0, & \pi_{\alpha\beta}^0 = 2\mu_p (\boldsymbol{\varepsilon}_{\alpha\beta}^{\mathbf{x}'}(\mathbf{w}^0) + \boldsymbol{\varepsilon}_{\alpha\beta}^{\mathbf{z}'}(\mathbf{w}^2)) + \lambda_p (\partial_{y_1} w_1^1 + \boldsymbol{\varepsilon}_{\gamma\gamma}^{\mathbf{x}'}(\mathbf{w}^0) + \boldsymbol{\varepsilon}_{\gamma\gamma}^{\mathbf{z}'}(\mathbf{w}^2)) \delta_{\alpha\beta}, & \text{in } Y, \\ \pi_{\alpha\beta}^0 n_\beta = 0 & \text{on } \partial Y, \end{cases} \quad (\text{B.18})$$

with \mathbf{w}^0 known from (B.10) and w_1^1 from (B.16) at this stage. It is easy to check that the solution of this boundary value problem is

$$\begin{cases} \pi_{\alpha\beta}^0 = 0, \\ w_\alpha^2 = -e_{\alpha\beta}^{\mathbf{x}'}(\mathbf{w}^0) z_\beta - \frac{\lambda_p}{2(\mu_p + \lambda_p)} z_\alpha \frac{\partial W_1}{\partial y_1}(y_1, \mathbf{x}') + \frac{\lambda_p}{2(\mu_p + \lambda_p)} g_\alpha + W_\alpha^2(y_1, \mathbf{x}') + \Omega^2(y_1, \mathbf{x}')(\mathbf{e}_1, \mathbf{z}', \mathbf{e}_\alpha), \end{cases} \quad (\text{B.19})$$

where

$$g_2 = \left(\frac{z_2^2}{2} - \frac{z_3^2}{2} \right) \frac{\partial^2 W_2^0}{\partial y_1^2} + z_2 z_3 \frac{\partial^2 W_3^0}{\partial y_1^2}, \quad g_3 = \left(\frac{z_3^2}{2} - \frac{z_2^2}{2} \right) \frac{\partial^2 W_3^0}{\partial y_1^2} + z_2 z_3 \frac{\partial^2 W_2^0}{\partial y_1^2}. \quad (\text{B.20})$$

The above form of w_α^2 along with w_α^0 in (B.10) can now be used to find $\pi_{11}^0 = (2\mu_p + \lambda_p) \partial_{y_1} w_1^1 + \lambda_p (\partial_{x_\alpha} w_\alpha^0 + \partial_{z_\alpha} w_\alpha^2)$, and we get

$$\pi_{11}^0 = E_p \left(\frac{\partial W_1}{\partial y_1}(y_1, \mathbf{x}') - \frac{\partial^2 W_\alpha^0}{\partial y_1^2}(y_1, \mathbf{x}') z_\alpha \right), \quad (\text{B.21})$$

266 where we used that $E_p = \mu_p(2\mu_p + 3\lambda_p)/(\mu_p + \lambda_p)$. It is now sufficient to remember that $\overline{\pi_{11}^0} = 0$ to
 267 get that $\partial_{y_1} W_1 = 0$, hence the above expression of π_{11}^0 simplifies to the form announced in (B.11)
 268 and w_1^1 in (B.16) simplifies to that in (B.11).

We now use the boundary value problem set in Y for the unknowns $(\pi_{1\alpha}^0, w_1^2)$. From $(E_1)^{-2}$ and $(C_{1\alpha})^0$ in (13), it reads as follows

$$\begin{cases} \partial_{z_\alpha} \pi_{1\alpha}^0 = 0, & \pi_{1\alpha}^0 = \mu_p (\partial_{y_1} w_\alpha^1 + \partial_{x_\alpha} w_1^0 + \partial_{z_\alpha} w_1^2), & \text{in } Y, \\ \pi_{1\alpha}^0 n_\alpha = 0, & \text{on } \partial Y, \end{cases} \quad (\text{B.22})$$

with w_1^0 known from (B.10) and w_α^1 from (B.17) at this stage. The solution is found to be of the form

$$\begin{cases} \pi_{1\alpha}^0 = \mu_p \frac{\partial \Omega^1}{\partial y_1}(y_1, \mathbf{x}')(\mathbf{e}_1, \mathbf{z}', \mathbf{e}_\alpha), \\ w_1^2 = W_1^2(y_1, \mathbf{x}') - z_\alpha \left(\frac{\partial W_\alpha^1}{\partial y_1}(y_1, \mathbf{x}') + \frac{\partial W_1^0}{\partial x_\alpha}(\mathbf{x}') \right), \end{cases} \quad (\text{B.23})$$

and we see that $\Omega^1 = 0$ implies $\pi_{1\alpha}^0 = 0$. To show that $\Omega^1 = 0$, we use $\partial_{y_1} \pi_{1\alpha}^0 + \partial_{z_\beta} \pi_{\alpha\beta}^1 = 0$ which we infer from $(E_\alpha)^{-1}$. Multiplying by $\mathbf{v} = v_\alpha \mathbf{e}_\alpha$ with the triple product $v_\alpha = (\mathbf{e}_1, \mathbf{z}', \mathbf{e}_\alpha)$ and integrating over Y , we find that

$$\int_Y v_\alpha \partial_{y_1} \pi_{1\alpha}^0 \, d\mathbf{z}' + \int_{\partial Y} v_\alpha \pi_{\alpha\beta}^1 n_\beta \, dl - \int_Y \partial_{z_\beta} v_\alpha \pi_{\alpha\beta}^1 \, d\mathbf{z}' = 0. \quad (\text{B.24})$$

Since $\boldsymbol{\pi}^1$ is symmetric and $\nabla \mathbf{v}$ is anti-symmetric, we have $\partial_{z_\beta} v_\alpha \pi_{\alpha\beta}^1 = 0$, and $\pi_{\alpha\beta}^1 n_\beta = 0$ on ∂Y . Hence, (B.24) reduces to

$$\int_Y v_\alpha \frac{\partial \pi_{1\alpha}^0}{\partial y_1} d\mathbf{z}' = 0, \quad \text{hence} \quad \frac{\partial^2 \Omega^1}{\partial y_1^2}(y_1, \mathbf{x}') \int_Y (\mathbf{e}_1, \mathbf{z}', \mathbf{e}_\alpha)^2 d\mathbf{z}' = 0. \quad (\text{B.25})$$

269 Next, with $(\mathbf{e}_1, \mathbf{z}', \mathbf{e}_\alpha)^2 = |\mathbf{z}'|^2$ whose integral does not vanish, we obtain that $\partial_{y_1} \Omega^1$ does not
 270 depend on y_1 ; anticipating that $\partial_{y_1} \Omega^1(\hat{h}, \mathbf{x}') = 0$ (see forthcoming (B.35)) and $\Omega^1(0, \mathbf{x}') = 0$ (see
 271 forthcoming (B.41)), we deduce that $\Omega^1 = 0$ everywhere. It follows that $\pi_{1\alpha}^0 = 0$, from (B.23),
 272 and that $w_\alpha^1 = W_\alpha^1(y_1, \mathbf{x}')$, from (B.17), in agreement with (B.11).

273 *Appendix B.1.5. Third step: $\overline{\pi_{1i}^1}$ in (B.12) and the Euler-Bernoulli equations in (B.13)*

This starts with (E)⁰ in (13) integrated over Y , specifically

$$\frac{\partial \overline{\pi_{11}^1}}{\partial y_1} + \rho_p \omega^2 \varphi W_1^0 = 0, \quad \frac{\partial \overline{\pi_{1\alpha}^1}}{\partial y_1} + \rho_p \omega^2 \varphi W_\alpha^0 = 0, \quad (\text{B.26})$$

274 where we have used that $\overline{\pi^0} = 0$ from (B.9) and (B.11) and $\boldsymbol{\pi}^2 \mathbf{n}_{\partial Y} = \mathbf{0}$. Since W_1^0 depends only
 275 on \mathbf{x}' and anticipating that $\overline{\pi_{11}^1}(\hat{h}, \mathbf{x}') = 0$ we obtain the form of $\overline{\pi_{11}^1}$ in (B.12) by integration of
 276 (B.26).

To get $\overline{\pi_{1\alpha}^1}$, we multiply (E)₁⁻¹ (which reads $\partial_{y_1} \pi_{11}^0 + \partial_{z_\beta} \pi_{1\beta}^1 = 0$, with π_{11}^0 in (B.11)) by z_α and integrate over Y to find that

$$E_p \frac{\partial^3 W_\beta^0}{\partial y_1^3}(y_1, \mathbf{x}') \int_Y z_\alpha z_\beta ds + \int_Y \pi_{1\beta}^1 \delta_{\alpha\beta} ds = 0, \quad (\text{B.27})$$

where we have used that $\pi_{1\beta}^1 n_{\beta 1 \partial Y} = 0$. For the circular cross-section of the beams, $\int_Y z_2 z_3 d\mathbf{z}' = 0$ and $\int_Y z_2^2 d\mathbf{z}' = \int_Y z_3^2 d\mathbf{z}' = \pi \hat{r}^4 / 4$. It follows that

$$\hat{S} \overline{\pi_{1\alpha}^1}(y_1, \mathbf{x}') = -E_p \frac{\pi \hat{r}^4}{4} \frac{\partial^3 W_\alpha^0}{\partial y_1^3}(y_1, \mathbf{x}'), \quad (\text{B.28})$$

in agreement with (B.12) (with $\varphi \hat{S} = \pi \hat{r}^2$). Coming back to (B.26) with the above form of $\overline{\pi_{1\alpha}^1}$, we deduce that

$$E_p \frac{\pi \hat{r}^4}{4} \frac{\partial^4 W_\alpha^0}{\partial y_1^4} - \rho_p \omega^2 \varphi \hat{S} W_\alpha^0 = 0, \quad (\text{B.29})$$

277 in agreement with (B.13).

278 *Appendix B.2. Effective boundary conditions at the top of the array of beams*

As we have done in (30), we consider the following expansions for the displacement and stress

$$\mathbf{u} = \sum_{n \geq 0} \eta^n \mathbf{v}^n(\mathbf{z}, \mathbf{x}'), \quad \boldsymbol{\sigma} = \sum_{n \geq 0} \eta^n \boldsymbol{\tau}^n(\mathbf{z}, \mathbf{x}'), \quad (\text{B.30})$$

with now $\mathbf{z} = (z_1, z_2, z_3)$. We use (e) in (33) which provides us with $\operatorname{div}_{\mathbf{z}} \boldsymbol{\tau}^0 = \operatorname{div}_{\mathbf{z}} \boldsymbol{\tau}^1 = \mathbf{0}$, and this makes the calculations identical to those conducted in §3.2 for the plates when integrating over $Z = \{z_1 \in (-\infty, 0), \mathbf{z}' \in Y\}$. We thus obtain

$$\overline{\pi_{1i}^0}(\hat{h}, \mathbf{z}', \mathbf{x}') = \overline{\pi_{1i}^1}(\hat{h}, \mathbf{z}', \mathbf{x}') = 0, \quad i = 1, 2, 3, \quad (\text{B.31})$$

(see (54)). The conditions on $\overline{\pi_{1i}^0}$ are consistent with (B.9) and (B.11). The condition on $\overline{\pi_{11}^1}$ is that anticipated to find (B.12). Eventually, the condition on $\overline{\pi_{1\alpha}^1}$ combined with (B.12) provides the conditions of zero shear force

$$\frac{\partial^3 W_\alpha^0}{\partial y_1^3}(\hat{h}, \mathbf{x}') = 0. \quad (\text{B.32})$$

To derive the condition of zero bending moment, we proceed in the same way as we have done in (B.24); with $\mathbf{v} = v_\alpha \mathbf{e}_\alpha$ and $v_\alpha = (\mathbf{e}_1, \mathbf{z}, \mathbf{e}_\alpha)$, we consider the vanishing integral $\int_Z v_\alpha \partial_{z_i} \tau_{i\alpha}^0 \, dv = 0$, hence

$$\int_{\partial Z} v_\alpha \tau_{i\alpha}^0 n_i = 0, \quad (\text{B.33})$$

where we have used that $\partial_{z_i} v_\alpha \tau_{i\alpha}^0 = 0$ by construction. Because $\boldsymbol{\tau}^0 \cdot \mathbf{n}$ vanishes on ∂Z except at the bottom face $z_1 = -z_m$ and passing to the limit $z_m \rightarrow +\infty$, this integral reduces to

$$\int_Y v_\alpha \pi_{1\alpha}^0(\hat{h}, \mathbf{z}', \mathbf{x}') \, ds = 0. \quad (\text{B.34})$$

Making use of (B.23) leads to the anticipated boundary condition

$$\frac{\partial \Omega^1}{\partial y_1}(\hat{h}, \mathbf{x}') = 0, \quad (\text{B.35})$$

that we have used to get $\pi_{1\alpha}^0 = 0$. It remains to derive the condition of zero bending moment. By considering $\mathbf{a} = z_\alpha \mathbf{e}_1 - z_1 \mathbf{e}_\alpha$ and integrating over Z the scalar $\mathbf{a} \cdot \operatorname{div}_{\mathbf{z}} \boldsymbol{\tau}^0$ (since $\operatorname{div}_{\mathbf{z}} \boldsymbol{\tau}^0 = \mathbf{0}$), we found that

$$0 = \int_{\partial Z} a_i \tau_{ij}^0 n_j \, ds = - \int_Y z_\alpha \tau_{11}^0|_{z_1=-z_m} \, ds - z_m \int_Y \tau_{1\alpha}^0|_{z_1=-z_m} \, ds, \quad (\text{B.36})$$

for $\alpha = 2, 3$. Since we have in addition $0 = \int_{\partial Z} \tau_{ij}^0 n_j \, ds = \int_Y \tau_{1\alpha}^0|_{z_1=-z_m} \, ds$, we can pass to the limit $z_m \rightarrow \infty$, and get $0 = \int_Y z_\alpha \tau_{11}^0 \rightarrow \overline{z_\alpha \pi_{11}^0}(\hat{h}, \mathbf{x}')$. Now accounting for π_{11}^0 in (B.21), we obtain the expected boundary condition

$$\frac{\partial^2 W_\alpha^0}{\partial y_1^2}(\hat{h}, \mathbf{x}') = 0. \quad (\text{B.37})$$

279 Appendix B.3. Effective transmission conditions between the substrate and the array of beams

In the vicinity of the interface between the substrate and the array of beams, we consider the same expansions as in (B.30), and at the dominant order, we still have $\operatorname{div}_{\mathbf{z}} \boldsymbol{\tau}^0 = \operatorname{div}_{\mathbf{z}} \boldsymbol{\tau}^1 = \mathbf{0}$. The calculations are identical to that conducted in §3.3 when integrating over $Z = \{z_1 \in (0, +\infty), \mathbf{z}' \in Y\} \cup \{z_1 \in (-\infty, 0), \mathbf{z}' \in (-\hat{\ell}/2, \hat{\ell}/2)^2\}$, and we find

$$\sigma_{1i}^0(0^-, \mathbf{x}') = 0, \quad i = 1, 2, 3, \quad (\text{B.38})$$

which are consistent with (B.9) and (B.11). Next, using $\overline{\pi_{1i}^1}$ in (B.12), we find

$$\sigma_{11}^1(0^-, \mathbf{x}') = \rho_p \omega^2 \varphi \hat{h} W_1^0(\mathbf{x}'), \quad \sigma_{1\alpha}^1(0^-, \mathbf{x}') = -E_p \frac{\pi \hat{r}^4}{4S} \frac{\partial^3 W_\alpha^0}{\partial y_1^3}(0, \mathbf{x}'). \quad (\text{B.39})$$

We have yet to establish the continuity of the displacement. From the counterpart of (c') in (42) (with $\mathbf{z}' \rightarrow \mathbf{z}$), it is easily seen that we have at the dominant orders

$$\boldsymbol{\varepsilon}^z(\mathbf{v}^0) = \boldsymbol{\varepsilon}^z(\mathbf{v}^1) = \mathbf{0}. \quad (\text{B.40})$$

Therefore \mathbf{v}^0 and \mathbf{v}^1 are piecewise rigid body motions, namely $\mathbf{v}^i = \hat{\boldsymbol{\Omega}}^i(\mathbf{x}') \times \mathbf{z} + \mathbf{V}^i(\mathbf{x}')$, $i = 0, 1$. Invoking the periodicity of \mathbf{v}^i , $i = 0, 1$ with respect to z_2 and z_3 for $z_1 < 0$ and the continuity of \mathbf{v}^i at $z_1 = 0$, these rigid body motions reduce to a single translation over Z , hence $\hat{\boldsymbol{\Omega}}^i = \mathbf{0}$. Using the matching conditions on the displacements, we obtain the conditions that we have anticipated (see (B.15) and (B.25)), namely

$$\boldsymbol{\Omega}^i(0, \mathbf{x}') = \hat{\boldsymbol{\Omega}}^i \cdot \mathbf{e}_1 = 0, \quad i = 0, 1, \quad (\text{B.41})$$

and the boundary conditions

$$u_1^0(0^-, \mathbf{x}') = W_1^0(\mathbf{x}'), \quad u_\alpha^0(0^-, \mathbf{x}') = W_\alpha^0(0^+, \mathbf{x}'), \quad \frac{\partial W_\alpha^0}{\partial z_1}(0^+, \mathbf{x}') = 0. \quad (\text{B.42})$$

280 Appendix B.4. The final problem

281 The effective problem (B.1) is obtained for $(\mathbf{u} = \mathbf{u}^0, \boldsymbol{\sigma} = \boldsymbol{\sigma}^0 + \eta \boldsymbol{\sigma}^1)$ in the substrate for
 282 $x_1 < 0$, $(\mathbf{u} = \mathbf{W}^0, \boldsymbol{\sigma} = \boldsymbol{\pi}^0 + \eta \boldsymbol{\pi}^1)$ and in the region of the array for $x_1 > 0$. Remembering that
 283 $y_1 = x_1/\eta$ and $\hat{h} = h/\eta$, $\hat{r} = r_p/\eta^2$, it is easy to see that (i) the Euler-Bernoulli equation in (B.1)
 284 is obtained from (B.13), (ii) the effective boundary conditions announced in (B.3) from (B.32),
 285 (B.37)-(B.39) and (B.42).

286 References

- 287 [1] H. Lamb, I. on the propagation of tremors over the surface of an elastic solid, Philosophical Transactions of the
 288 Royal Society of London. Series A, 203 (359-371) (1904) 1–42.
 289 [2] C. Pekeris, The seismic surface pulse, Proceedings of the national academy of sciences of the United States of
 290 America 41 (7) (1955) 469.
 291 [3] P. C. Jennings, J. Bielak, Dynamics of building-soil interaction, Bulletin of the seismological society of America
 292 63 (1) (1973) 9–48.
 293 [4] E. Kausel, R. V. Whitman, J. P. Morray, F. Elsabee, The spring method for embedded foundations, Nuclear Engi-
 294 neering and design 48 (2-3) (1978) 377–392.
 295 [5] G. Gazetas, Formulas and charts for impedances of surface and embedded foundations, Journal of geotechnical
 296 engineering 117 (9) (1991) 1363–1381.
 297 [6] E. Kausel, Early history of soil–structure interaction, Soil Dynamics and Earthquake Engineering 30 (9) (2010)
 298 822–832.
 299 [7] J. E. Luco, L. Contesse, Dynamic structure-soil-structure interaction, Bulletin of the Seismological Society of
 300 America 63 (4) (1973) 1289–1303.
 301 [8] H. Wong, M. Trifunac, Two-dimensional, antiplane, building-soil-building interaction for two or more buildings
 302 and for incident planet sh waves, Bulletin of the Seismological Society of America 65 (6) (1975) 1863–1885.
 303 [9] A. Wirgin, P.-Y. Bard, Effects of buildings on the duration and amplitude of ground motion in mexico city, Bulletin
 304 of the Seismological Society of America 86 (3) (1996) 914–920.
 305 [10] P. Guéguen, P. Bard, J. Semblat, Engineering seismology: seismic hazard and risk analysis: seismic hazard analysis
 306 from soil-structure interaction to site-city interaction, in: Proc. 12th World Conference on Earthquake Engineering,
 307 2000.

- 308 [11] D. Clouteau, D. Aubry, Modifications of the ground motion in dense urban areas, *Journal of Computational Acoustics* 9 (04) (2001) 1659–1675.
- 309
- 310 [12] C. Tsogka, A. Wirgin, Simulation of seismic response in an idealized city, *Soil Dynamics and Earthquake Engineering* 23 (5) (2003) 391–402.
- 311
- 312 [13] P. Gueguen, P.-Y. Bard, Soil-structure and soil-structure-soil interaction: experimental evidence at the volvi test site, *Journal of Earthquake Engineering* 9 (05) (2005) 657–693.
- 313
- 314 [14] M. Kham, J.-F. Semblat, P.-Y. Bard, P. Dangla, Seismic site–city interaction: main governing phenomena through simplified numerical models, *Bulletin of the Seismological Society of America* 96 (5) (2006) 1934–1951.
- 315
- 316 [15] J.-P. Groby, A. Wirgin, Seismic motion in urban sites consisting of blocks in welded contact with a soft layer overlying a hard half-space, *Geophysical Journal International* 172 (2) (2008) 725–758.
- 317
- 318 [16] K. Uenishi, The town effect: dynamic interaction between a group of structures and waves in the ground, *Rock mechanics and rock engineering* 43 (6) (2010) 811–819.
- 319
- 320 [17] M. Todorovska, M. Trifunac, The system damping, the system frequency and the system response peak amplitudes during in-plane building–soil interaction, *Earthquake engineering & structural dynamics* 21 (2) (1992) 127–144.
- 321
- 322 [18] P. Gueguen, P.-Y. Bard, F. J. Chavez-García, Site-city seismic interaction in mexico city–like environments: an analytical study, *Bulletin of the Seismological Society of America* 92 (2) (2002) 794–811.
- 323
- 324 [19] C. Boutin, P. Roussillon, Assessment of the urbanization effect on seismic response, *Bulletin of the Seismological Society of America* 94 (1) (2004) 251–268.
- 325
- 326 [20] M. Ghergu, I. R. Ionescu, Structure–soil–structure coupling in seismic excitation and city effect, *International Journal of Engineering Science* 47 (3) (2009) 342–354.
- 327
- 328 [21] C. Boutin, P. Roussillon, Wave propagation in presence of oscillators on the free surface, *International journal of engineering science* 44 (3-4) (2006) 180–204.
- 329
- 330 [22] L. Schwan, C. Boutin, Unconventional wave reflection due to resonant surface, *Wave Motion* 50 (4) (2013) 852–868.
- 331
- 332 [23] C. Boutin, L. Schwan, M. S. Dietz, Elastodynamic metasurface: Depolarization of mechanical waves and time effects, *Journal of Applied Physics* 117 (6) (2015) 064902.
- 333
- 334 [24] L. Schwan, C. Boutin, L. Padrón, M. Dietz, P.-Y. Bard, C. Taylor, Site-city interaction: theoretical, numerical and experimental crossed-analysis, *Geophysical Journal International* 205 (2) (2016) 1006–1031.
- 335
- 336 [25] E. Garova, A. Maradudin, A. Mayer, Interaction of rayleigh waves with randomly distributed oscillators on the surface, *Physical Review B* 59 (20) (1999) 13291.
- 337
- 338 [26] H. Wegert, E. A. Mayer, L. M. Reindl, W. Ruile, A. P. Mayer, Interaction of saws with resonating structures on the surface, in: 2010 IEEE International Ultrasonics Symposium, IEEE, 2010, pp. 185–188.
- 339
- 340 [27] A. Maznev, V. Gusev, Waveguiding by a locally resonant metasurface, *physical Review B* 92 (11) (2015) 115422.
- 341
- 342 [28] A. Maznev, Bifurcation of avoided crossing at an exceptional point in the dispersion of sound and light in locally resonant media, *Journal of Applied Physics* 123 (9) (2018) 091715.
- 343
- 344 [29] S. Kuznetsov, Seismic waves and seismic barriers, *Acoustical Physics* 57 (3) (2011) 420–426.
- 345
- 346 [30] S.-H. Kim, M. P. Das, Seismic waveguide of metamaterials, *Modern Physics Letters B* 26 (17) (2012) 1250105.
- 347
- 348 [31] S.-H. Kim, M. P. Das, Artificial seismic shadow zone by acoustic metamaterials, *Modern Physics Letters B* 27 (20) (2013) 1350140.
- 349
- 350 [32] S. Brûlé, E. Javelaud, S. Enoch, S. Guenneau, Experiments on seismic metamaterials: molding surface waves, *Physical review letters* 112 (13) (2014) 133901.
- 351
- 352 [33] S. Krödel, N. Thomé, C. Daraio, Wide band-gap seismic metastructures, *Extreme Mechanics Letters* 4 (2015) 111–117.
- 353
- 354 [34] A. Colombi, P. Roux, S. Guenneau, P. Gueguen, R. V. Craster, Forests as a natural seismic metamaterial: Rayleigh wave bandgaps induced by local resonances, *Scientific reports* 6 (2016) 19238.
- 355
- 356 [35] G. Carta, I. Jones, N. Movchan, A. Movchan, M. Nieves, Gyro-elastic beams for the vibration reduction of long flexural systems, *Proceedings of the Royal Society A: Mathematical, Physical and Engineering Sciences* 473 (2203) (2017) 20170136.
- 357
- 358 [36] D. Colquitt, A. Colombi, R. Craster, P. Roux, S. Guenneau, Seismic metasurfaces: Sub-wavelength resonators and rayleigh wave interaction, *Journal of the Mechanics and Physics of Solids* 99 (2017) 379–393.
- 359
- 360 [37] A. Maurel, J.-J. Marigo, K. Pham, S. Guenneau, Conversion of love waves in a forest of trees, *Physical Review B* 98 (13) (2018) 134311.
- 361
- 362 [38] A. Palermo, A. Marzani, Control of love waves by resonant metasurfaces, *Scientific reports* 8 (1) (2018) 7234.
- 363
- 364 [39] A. Palermo, F. Zeighami, A. Marzani, Seismic metasurfaces for love waves control, in: EGU General Assembly Conference Abstracts, Vol. 20, 2018, p. 18607.
- 365
- 366 [40] L. Kelders, J. F. Allard, W. Lauriks, Ultrasonic surface waves above rectangular-groove gratings, *The Journal of the Acoustical Society of America* 103 (5) (1998) 2730–2733.
- [41] J. Zhu, Y. Chen, X. Zhu, F. J. Garcia-Vidal, X. Yin, W. Zhang, X. Zhang, Acoustic rainbow trapping, *Scientific reports* 3 (2013) 1728.

- 367 [42] J. Pendry, L. Martin-Moreno, F. Garcia-Vidal, Mimicking surface plasmons with structured surfaces, *science*
368 305 (5685) (2004) 847–848.
- 369 [43] F. Garcia-Vidal, L. Martin-Moreno, J. Pendry, Surfaces with holes in them: new plasmonic metamaterials, *Journal*
370 *of optics A: Pure and applied optics* 7 (2) (2005) S97.
- 371 [44] P. G. Ciarlet, P. Destuynder, A justification of the two-dimensional linear plate model, *J Mec* 18 (2) (1979) 315–344.
- 372 [45] D. Caillerie, Plaques élastiques minces à structure périodique de période et d'épaisseurs comparables *Sc. Paris Sér.*
373 *II* 294 (1982) 159–162.
- 374 [46] L. Trabucho, J. Viano, Derivation of generalized models for linear elastic beams by asymptotic expansion methods,
375 *Applications of Multiple Scaling in Mechanics* (1987) 302–315.
- 376 [47] G. Geymonat, F. Krasucki, J.-J. Marigo, Sur la commutativité des passages à la limite en théorie asymptotique des
377 poutres composites, *Comptes rendus de l'Académie des sciences. Série 2, Mécanique, Physique, Chimie, Sciences*
378 *de l'univers, Sciences de la Terre* 305 (4) (1987) 225–228.
- 379 [48] B. Miara, L. Trabucho, Approximation spectrale pour une poutre en élasticité linéarisée, *Comptes rendus de*
380 *l'Académie des sciences. Série 1, Mathématique* 311 (10) (1990) 659–662.
- 381 [49] G. Corre, A. Lebé, K. Sab, M. K. Ferradi, X. Céspedes, Higher-order beam model with eigenstrains: theory and
382 illustrations, *ZAMM-Journal of Applied Mathematics and Mechanics/Zeitschrift für Angewandte Mathematik und*
383 *Mechanik* 98 (7) (2018) 1040–1065.
- 384 [50] R. Abdelmoula, J.-J. Marigo, The effective behavior of a fiber bridged crack, *Journal of the Mechanics and Physics*
385 *of Solids* 48 (11) (2000) 2419–2444.
- 386 [51] M. David, J.-J. Marigo, C. Pideri, Homogenized interface model describing inhomogeneities located on a surface,
387 *Journal of Elasticity* 109 (2) (2012) 153–187.
- 388 [52] J.-J. Marigo, A. Maurel, Homogenization models for thin rigid structured surfaces and films, *The Journal of the*
389 *Acoustical Society of America* 140 (1) (2016) 260–273.
- 390 [53] A. Maurel, K. Pham, J.-J. Marigo, Scattering of gravity waves by a periodically structured ridge of finite extent,
391 *Journal of Fluid Mechanics* 871 (2019) 350–376.
- 392 [54] A. Maurel, J.-J. Marigo, J.-F. Mercier, K. Pham, Modelling resonant arrays of the helmholtz type in the time
393 domain, *Proceedings of the Royal Society A: Mathematical, Physical and Engineering Sciences* 474 (2210) (2018)
394 20170894.
- 395 [55] A. Maurel, K. Pham, Multimodal method for the scattering by an array of plates connected to an elastic half-space,
396 *The Journal of the Acoustical Society of America* 146 (6) (2019) 4402–4412.
- 397 [56] J. Achenbach, *Wave propagation in elastic solids*, Vol. 16, Elsevier, 2012.